



Horizon 2020  
Programme

**CORTEX**

*Research and Innovation Action (RIA)*

This project has received funding from the European Union's Horizon 2020 research and innovation programme under grant agreement No 754316.

Start date : 2017-09-01 Duration : 48 Months  
<http://cortex-h2020.eu>



---

**Methodology for uncertainty and sensitivity analysis**

---

Authors : Ms. Soobeen YUM (TU Muenchen), Rafael Macian (TUM), Paolo Vinai (Chalmers)

CORTEX - Contract Number: 754316

Project officer: Foivos MARIAS

Document title	Methodology for uncertainty and sensitivity analysis
Author(s)	Ms. Soobeen YUM, Rafael Macian (TUM), Paolo Vinai (Chalmers)
Number of pages	40
Document type	Deliverable
Work Package	WP01
Document number	D1.1
Issued by	TU Muenchen
Date of completion	2019-06-25 09:32:23
Dissemination level	Public

## Summary

A basic methodology for the uncertainty propagation and the sensitivity analysis has been developed for neutron noise simulations. The methodology is tested on a hypothetical case in which a density fluctuation occurs in the UO<sub>2</sub> fuel rods of the zero-power research reactor CROCUS. The nuclear data are prepared with the Monte-Carlo code Serpent, while the neutron noise calculations are performed with the code CORE SIM. A total of 26 main design and operating parameters are sorted considering the target reactor and event, then, the samples are generated following the distribution of each parameter. Through a series of Serpent computations with generated input matrices, the required inputs for CORE SIM are obtained. For the input uncertainty propagation, two approaches, namely Wilks' formula and the Monte-Carlo technique are considered: first and fourth order tolerance intervals provided by Wilks' formula show the results of 95%/95% tolerance limit, while 95% upper and lower confidence limit values are identified from the Monte-Carlo approach, which creates an empirical probability distribution for the output variable of interest. For the Monte-Carlo computations, the total number of sample sets is substantially increased with the aid of surrogate modelling. The results from these two different approaches are then compared to each other, so as to check the differences in terms of conservatism. Additionally, by means of the space mapping of the neutron noise uncertainties, it is shown that their magnitude has a spatial dependency, unlike the phase of the neutron noise. Additionally, the correlation-based approach and the variance-based approach are selected to carry out a sensitivity analysis considering the complexity of the perturbed neutron flux behavior. The sensitivity corresponding to the clad thickness shows the largest value in terms of both main index and total index for the magnitude of the neutron noise. However, all the first order indices have a value less than 0.05 and the total order indices are broadly similar in case of the phase of the neutron noise. In other words, no parameter has a strong direct effect on the output result but shapes an influence only by the collaboration with other parameters. In addition, a methodology based on spectral/frequency decomposition is discussed for the analysis of oscillatory phenomena in nuclear reactors.

## Approval

Date	By
2019-06-25 09:40:20	Dr. Paolo VINAI (Chalmers)

## Table of Contents

1	Overview of the Methodology for Uncertainty and Sensitivity Analysis .....	4
2	Uncertainty Propagation and Sensitivity Analysis .....	5
2.1	Preparation for the Analysis .....	5
2.2	Uncertainty Propagation .....	13
2.3	Sensitivity Analysis .....	19
3	Analysis of Nuclear Oscillatory Phenomena using Spectral / Frequency Decomposition .....	26
3.1	Basis of the Methodology .....	26
3.2	The Application of the FFT on the Global Parameter Reactor Power .....	27
3.3	The Application of the FFT to Local Physical Parameters .....	30
3.4	Phase Shift Determination between Oscillating Parameters .....	36
4	Conclusions .....	38
5	References .....	39

## Index of Tables

Table 1: High priority parameters affecting the neutron noise .....	7
Table 2: The uncertainty range and distribution of input parameter .....	9
Table 3: Few-group constant generation summary .....	11
Table 4: Minimum number of calculations for two-sided statistical tolerance limits .....	15
Table 5: Shapiro-Wilks test for normality p-value for neutron noise data .....	16

## Table of Figures

Figure 1: Flow chart of the developed methodology .....	4
Figure 2: Serpent regions for cross-section homogenization in the CROCUS reactor .....	11
Figure 3: The sequence of codes computation .....	12
Figure 4: Modelled reactor core in CORE SIM .....	13
Figure 5: Probability density function for neutron noise data .....	17
Figure 6: Uncertainty range estimated with different approaches .....	18
Figure 7: The trends on the range of the noise uncertainty range in radial direction of the core (axial level $k = 15$ ) .....	19
Figure 8: Normalized noise uncertainty by the static neutron flux .....	19
Figure 9: Spearman rank and partial correlation coefficients for neutron noise data .....	22
Figure 10: Comparison of statistical error from 'Jansen 1999' and 'Sobol 2007' at increasing number of model runs .....	23
Figure 11: Variance-based sensitivity indices for neutron noise data; first order sensitivity index (left) and total sensitivity index (right) .....	25
Figure 12: Section of a feedwater transient in a BWR with an unbounded power oscillation: Total Reactor Power .....	28
Figure 13: Spectral analysis of the power signal in Figure 12. The signal is characterized by a high amplitude with a frequency of $f = 0$ Hz resulting from the offset, that is, the mean value of the input signal .....	28
Figure 14: Power signal and fitted polynomial of 1 <sup>st</sup> grade (linear fitting): the average value of the signal is then represented by the green line, which, because the power rises steadily with time has a positive slope with time. ....	29
Figure 15: Oscillatory component of the power signal after the linearly growing average value is subtracted. The signal is then ready to be spectrally processed. ....	29





Figure 16: Spectral analysis of the oscillation signal ..... 30

Figure 17: Input signals of two adjacent cells in a 3-D x-y-z model of the BWR core during a feedwater transient event ..... 31

Figure 18: Spectral analysis of the unprocessed mass flow rate signals for the two the adjacent core cells of Figure 17 ..... 31

Figure 19: Identification of the oscillatory and non-oscillatory part of the mass flow rate signals shown in Figure 17. The 1<sup>st</sup> order fitting shows the growing trend of the mass flow rate in both cells and indicates the faster variation of the one corresponding to (x = 15, y = 11, z = 6). ..... 32

Figure 20: Processed signals. Only the oscillatory part is considered for the spectral analysis. .... 32

Figure 21: Spectral analysis of the oscillation signal of two adjacent cells ..... 33

Figure 22: Radial spectral analysis of the mass flow rate signal for core level 6. .... 34

Figure 23: Expanded central section of Figure 22. The cells (eventually fuel assemblies) driving the oscillatory feed-back behavior in the core are clearly identified by the high amplitudes about the 0.5 Hz frequency. Other fuel assemblies contribute much less or not at all to the power oscillations observed. .... 35

Figure 24: Axial amplitude spectra for the fuel assemblies in an X-Y central core plane. The large influence of the central channel on the power oscillations, which are driven by the oscillations in mass flow rates, is clearly seen. .... 35

Figure 25: Time dependent signal and processing for three reactor feed-back coupled variables. Above: full values. Below: processed signal with only the oscillatory components. .... 36

Figure 26: Spectral analysis of the three signals in Figure 25. A dominant frequency in the three cases show a clear coupling between the power and the mass flow rate with a frequency about 0.4 Hz for the dominant channels. The phase shifts (see figure below) show that the oscillations are happening through time-delayed feedback mechanisms as is expected physically in these types of oscillations. .... 37

Figure 27: Time domain reconstruction of the signals. The plots above show the consistency of the methodology. The plots below show the phase shifts for the most influential frequency at about 0.4 Hz. .... 37

## Abbreviations

UP	Uncertainty propagation
SA	Sensitivity analysis
UO <sub>2</sub>	Uranium oxide
U <sub>metal</sub>	Metallic uranium
SRS	Simple random sampling
PDF	Probability density function
MSE	Mean squared error
TUM	Technical University of Munich
FFT	Fast Fourier transform
DFT	Discrete Fourier transform
IFFT	Inverse fast Fourier transform

## Summary

A basic methodology for the uncertainty propagation and the sensitivity analysis has been developed for neutron noise simulations. The methodology is tested on a hypothetical case in which a density fluctuation occurs in the UO<sub>2</sub> fuel rods of the zero-power research reactor CROCUS. The nuclear data are prepared with the Monte-Carlo code Serpent, while the neutron noise calculations are performed with the code CORE SIM. A total of 26 main design and operating parameters are sorted considering the target reactor and event, then, the samples are generated following the distribution of each parameter. Through a series of Serpent computations with generated input matrices, the required inputs for CORE SIM are obtained.

For the input uncertainty propagation, two approaches, namely Wilks' formula and the Monte-Carlo technique are considered: first and fourth order tolerance intervals provided by Wilks' formula show the results of 95%/95% tolerance limit, while 95% upper and lower confidence limit values are identified from the Monte-Carlo approach, which creates an empirical probability distribution for the output variable of interest. For the Monte-Carlo computations, the total number of sample sets is substantially increased with the aid of surrogate modelling. The results from these two different approaches are then compared to each other, so as to check the differences in terms of conservatism. Additionally, by means of the space mapping of the neutron noise uncertainties, it is shown that their magnitude has a spatial dependency, unlike the phase of the neutron noise. Additionally, the correlation-based approach and the variance-based approach are selected to carry out a sensitivity analysis considering the complexity of the perturbed neutron flux behavior. The sensitivity corresponding to the clad thickness shows the largest value in terms of both main index and total index for the magnitude of the neutron noise. However, all the first order indices have a value less than 0.05 and the total order indices are broadly similar in case of the phase of the neutron noise. In other words, no parameter has a strong direct effect on the output result but shapes an influence only by the collaboration with other parameters.

In addition, a methodology based on spectral/frequency decomposition is discussed for the analysis of oscillatory phenomena in nuclear reactors.

# 1 Overview of the Methodology for Uncertainty and Sensitivity Analysis

The aim of Uncertainty Propagation (UP) is to identify and characterize all the potentially important input uncertainty parameters as well as the methodology to quantify the output variability due to the combination of these uncertainties. Besides in the nuclear safety field, a quantification of the uncertainties in computer calculations is generally desirable and often necessary in many other applications as well.

The Sensitivity Analysis (SA) allows to study how the uncertainty in the output of a model can be apportioned to different sources of uncertainty in the model input [1]. It may be used to determine the most contributing input variables to an output behaviour as the non-influential inputs, or to ascertain some interaction effects within the model.

This report describes the methodology on UP and SA that is developed for neutron noise simulations within the CORTEX project. The methodology is tested on the hypothetical case of an absorber of variable strength in the research reactor CROCUS. The nuclear data needed for the modelling of the reactor core are generated with the Monte-Carlo code Serpent [2] and the neutron noise simulations are performed using the neutron noise tool CORE SIM [3]. This document includes the relevant results from the test.

Figure 1 shows a schematic flow chart of the developed methodology. The initial five steps from the selection of the ‘target reactor’ and ‘target event’ to ‘output uncertainty treatment’ are shared in both uncertainty and sensitivity analyses. Therefore, these steps will be discussed in Section 2.1. Afterwards, Sections 2.2 and 2.3 will cover the detailed process on UP and SA, respectively.

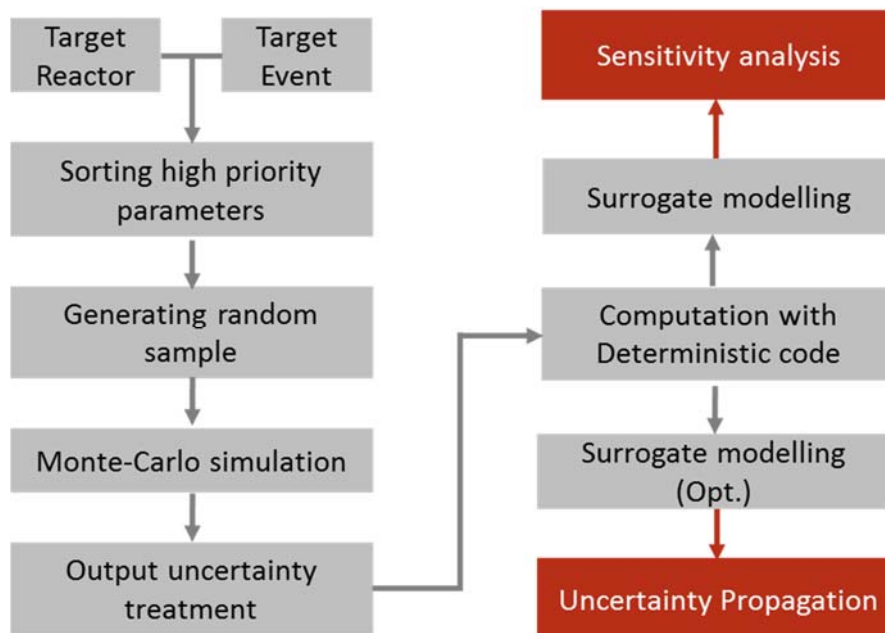


**Figure 1: Flow chart of the developed methodology**

## 2 Uncertainty Propagation and Sensitivity Analysis

### 2.1 Preparation for the Analysis

#### 2.1.1 Target Reactor

CROCUS is a research reactor at EPFL (École Polytechnique Fédérale de Lausanne) in Switzerland and is selected as a target reactor in this study. CROCUS is a zero-power reactor, with a maximum allowed power of 100 W [4]. The core is approximately cylindrical in shape with a diameter of about 60 cm and a height of 100 cm. There are two different kinds of fuel rods within the two fuel zones of the core. The central zone is fuelled with uranium dioxide (UO<sub>2</sub>) fuel rods and the peripheral zone is loaded with metallic uranium (U<sub>metal</sub>) fuel rods. The reactivity in the CROCUS reactor is controlled by the water level.

#### 2.1.2 Target Event

The case of an absorber of variable strength is selected as a representative neutron noise event for the analysis.

##### 2.1.2.1 Absorber of Variable Strength

An absorber of variable strength corresponds to the fluctuation of the neutron absorptions at selected locations in the system and is modelled with the fluctuation of the neutron macroscopic cross-sections at the location of the neutron noise source. Since the mathematical treatment as well as modelling of this case are easier than those of other sources, it is then selected as an initial trial case to develop the basic methodologies.

Here, an arbitrary event is considered in which the UO<sub>2</sub> fuel density is oscillating between 100% and 120% of its nominal value at a frequency of 1 Hz. This event describes the density change in all the 336 UO<sub>2</sub> fuel rods.

#### 2.1.3 Sorting High Priority Parameters

##### 2.1.3.1 Phenomena Identification under neutron flux oscillations

A phenomena identification is a systematic and documented way of gathering information on a specific subject, in order to determine what has the priority for the research on that subject. The 'Phenomena' here can actually be the condition of a particular reactor, system, component, a physical or engineering approximation, a reactor parameter, or anything else that might influence the figure-of-merit [5].

The code CORE SIM solves the neutron noise balance equations in the frequency domain and is based on 2-group neutron diffusion theory. The neutron noise balance equations implemented in CORE SIM could be written in a matrix form as reported below.

$$L\delta\phi = \delta S \quad (1)$$

$L$  describes the coefficient matrix, which depends on the frequency of the noise source, the neutron diffusion coefficients, the kinetics parameters and the static cross-sections of the system. The noise source term,  $\delta S$ , signifies the neutron noise source which results from either the fluctuations of the external neutron source around its mean value (if the system is subcritical and driven by an external neutron source), or from the fluctuations of the macroscopic cross-sections around their mean value.



### 2.1.3.2 *Sorting the parameters for each phenomenon*

As a result of the phenomena identification process, all the possible parameters which affect  $L$  and  $\delta S$  are investigated based on expert judgement and are described in Table 1.

### 2.1.4 *Random Samples Generation*

Considering the character and the condition of the target reactor, the applicable parameters are condensed and tabulated with their distribution data in Table 2. The parameters under normal distribution are considered as having a truncated normal distribution within the upper and lower design boundary values.

A total of 500 different sets of values for the uncertain parameters are generated with the Simple Random Sampling (SRS) method using a program developed in MATLAB. These sets are then used as inputs for a series of computations with Serpent in order to create sets of 2-energy group macroscopic cross-sections needed for the CORE SIM calculations.

For the uncertainty propagation, two different approaches using Wilks' formula and Monte-Carlo simulation, respectively, are considered. For the approach with Wilks' formula, 93 and 260 cases are extracted randomly from the pre-calculated 500 sets and used for the uncertainty propagation. The number of 93 and 260 stand for the required number of code runs at 1<sup>st</sup> order and 4<sup>th</sup> order Wilks' formula, respectively. The detailed information regarding Wilks' formula can be found in section 2.2.1.

Meanwhile, the Monte-Carlo approach can be used to build an empirical Probability Density Function (PDF), which is described in section 2.2.2.3. However, the total number of samples is requested to be large enough to decrease the uncertainty of the obtained PDF and generally needs to be larger than 10,000 cases. Therefore, the total number of sample sets is increased with the aid of surrogate modelling from 500 to 20,000 in order to have a more realistic estimation.

**Table 1: High priority parameters affecting the neutron noise**

Phenomenon Description		Key Parameters	
Diffusion coefficients		Initial pool temperature	
Effective delayed neutron fraction/ Decay constant		U-235 homogeneity	
		U-235 loading per rod	
		Control rod displacement	
		Water level	
		Control rod chemical composition	
Initial static flux	-	Total power	
		Fuel heated area	
	Peaking factor	Control rod displacement (radial direction)	
		Control rod displacement (axial direction)	
	Isotopic composition (Manufacturing tolerance)	U-235 homogeneity	
		U-235 loading per rod	
Neutron energy flux spectrum <sup>1</sup>	Factors in six factor formula	Thermal utilization factor ( $f$ )	Water level
			Initial position of control rods
			Control rods chemical composition
			Water level

<sup>1</sup> Here, the neutron energy flux spectrum is considered as one of the main phenomena because of its contribution to the condensation of the cross-sections ( $\Sigma_x$ ).





		U-235 homogeneity
		U-235 loading per rod
		Fuel burnup (U-235 content during whole cycle)
	Resonance escape probability ( $p$ )	Fuel diameter
		Cladding thickness
		Filler gap thickness
	Fast fission factor ( $\epsilon$ )	Fuel diameter
		Cladding thickness
		Filler gap thickness
		U-235 enrichment
	Reproduction factor ( $\eta$ )	Composition of the fuel (Ratio between U-235 and U-238)
	Neutron speed (Average fast neutron speed/ Average thermal neutron speed)	Total power
		Initial pool temperature
	Noise source	Depends on the target event (Void generation, fuel rods displacement, etc)



**Table 2: The uncertainty range and distribution of input parameter**

No.	Parameter		Distribution	Unit	Mean	Standard deviation (Lower/Upper limit <sup>2</sup> )	Correlation with other parameters <sup>3</sup>
1	Water level		Normal	cm	95.22	0.01	
2	Initial pool temperature		Normal	°C	20.0	0.02	
3	Initial pool density		-	g/cm <sup>3</sup>			-2E-4* <2> + 1.0023
4	Fuel density	UO <sub>2</sub>	Normal	g/cm <sup>3</sup>	10.556	0.034	
5		U <sub>metal</sub>	Normal	g/cm <sup>3</sup>	18.677	0.044	
6	Nuclide mass fraction	U-235 of UO <sub>2</sub>	Normal	-	1.806E-2	7E-6	
7		U-238 of UO <sub>2</sub>	-	-			0.881513 - <6>
8		U-235 of U <sub>metal</sub>	Normal	-	9.470E-3	7E-6	
9		U-238 of UO <sub>2</sub>	-	-			1 - <8>
10	Active fuel length		Normal	cm	100.0	0.02	
11	Relative axial location	Bottom of upper Grid	-	cm			<10> + 0.5
12		Bottom of Upper Cd	-	cm			<10> + 1.0
13		Top of Upper Cd	-	cm			<10> + 1.05
14		Top of Upper Grid	-	cm			<10> + 2.55
15		Fuel rod top spring	-	cm			<10> + 1.47
16	Fuel diameter	Fuel rod outer surface of UO <sub>2</sub>	Normal	cm	0.526	8.5E-4	

<sup>2</sup> This column shows the value of lower and upper limit in case of having uniform distribution.

<sup>3</sup> <k> represents the parameter consistently with the ID numbers given in the first column.



17		Cladding outer surface of UO <sub>2</sub>	Normal	cm	0.63	5E-3	
18		Fuel rod outer surface of U <sub>metal</sub>	Normal	cm	0.85	1E-3	
19		Cladding outer surface of U <sub>metal</sub>	Uniform	cm	0.965	0.965 / 0.97	
20	Cladding thickness	UO <sub>2</sub>	Normal	cm	0.085	5E-3	
21		U <sub>metal</sub>	Normal	cm	0.1	5E-3	
22	Inner surface of cladding	UO <sub>2</sub>	-	cm			<17> - <20>
23		U <sub>metal</sub>	-	cm			<19> - <21>
24	Square pitch	UO <sub>2</sub>	Normal	cm	1.837	2E-4	
25		U <sub>metal</sub>	Normal	cm	2.917	2E-4	
26	Initial position of control rod		Uniform	cm	0.0	0.0 / 0.01	

### 2.1.5 Neutronics Data Generation using Serpent

The Serpent model of the CROCUS reactor has been built specifically for cross-section generation purposes [6]. Table 3 summarizes the main condition for the computation and Figure 2 shows both the axial and radial planes which are modelled in Serpent. The calculation is performed with 150 active cycles of  $10^5$  source neutrons, skipping the first 100 cycles.

**Table 3: Few-group constant generation summary**

Lattice physics code	Serpent v2.1.30
Number of cross-section sets	7
Energy structure	Two-group
Delayed neutron precursor groups	8
Nuclear data library	JEFF-3.1.1 at 300 K
Reactivity feedback	Not required

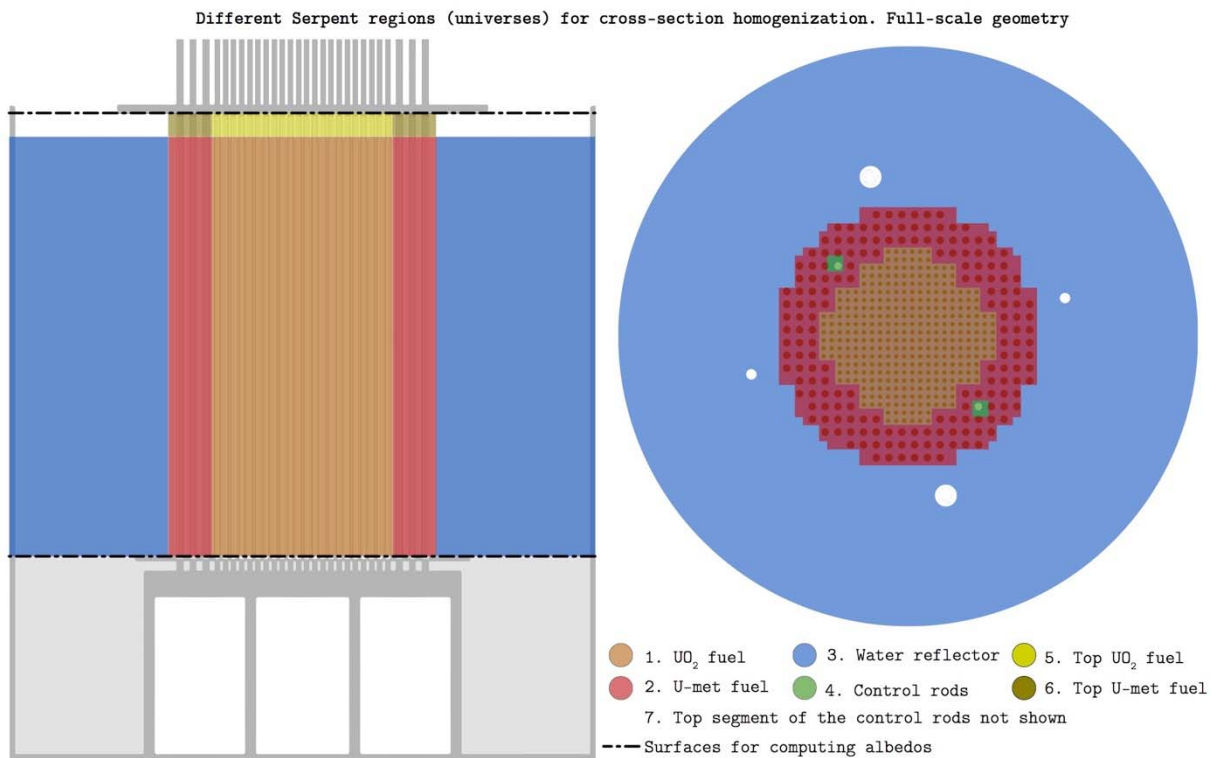


**Figure 2: Serpent regions for cross-section homogenization in the CROCUS reactor**

### 2.1.6 Output Uncertainty Treatment

#### 2.1.6.1 Combining Uncertainties

Serpent is a Monte-Carlo particle transport code, whose output provides a probability distribution with its mean value and the relative error for each variable of interest. Therefore, a proper uncertainty treatment must be carried out in case of an arithmetic operation with the output values.

#### Post-processing with fission cross-section data

In CORE SIM the perturbation of the macroscopic fission cross-section ( $\delta\Sigma_f$ ) is multiplied by the average number of neutrons released per fission event ( $\nu$ ). Serpent provides the error distributions



for both  $\delta\Sigma_f$  and  $v$ . Such information is combined to obtain an error distribution for the multiplication of two parameters as described below [7].

$$z = xy \tag{2}$$

$$\Delta z = |xy| \sqrt{\left(\frac{\Delta x}{x}\right)^2 + \left(\frac{\Delta y}{y}\right)^2} \tag{3}$$

Perturbation of macroscopic cross-sections for an absorber of variable strength

The perturbation of a generic macroscopic cross-section ( $\delta\Sigma_x$ ) is a crucial input for the CORE SIM neutron noise computation. In the case of an absorber of variable strength, the amplitude of the perturbation can be taken as the difference between two values: the one in perturbed conditions and the one in unperturbed conditions. Since both values have their own distributions from the Serpent computation, an additional error propagation is required to get the distribution for the difference of the two values and it is described below [7].

$$z = x - y \tag{4}$$

$$\Delta z = \sqrt{(\Delta x)^2 + (\Delta y)^2} \tag{5}$$

Here,  $x$  and  $y$  denote the mean values, and  $\Delta x$ ,  $\Delta y$  denote the relative errors.

2.1.6.2 Resampling Output Data for Further Uncertainty Propagation with CORE SIM

As mentioned in 2.1.6.1, the output data from Serpent computation is obtained as a distribution not as a discrete value. Therefore, it is necessary to define one representative value to assign this as an input for the further CORE SIM computation.

First of all, an arbitrary normal distribution with the Serpent-calculated mean and error values is made for all neutronics parameters of interest using MATLAB. Afterwards, one random value is selected by means of the SRS method. The obtained values are saved in the appropriate format to be recognized by CORE SIM.

Figure 3 summarizes the sequence of the computational codes applied for this study and the corresponding goals at each stage.

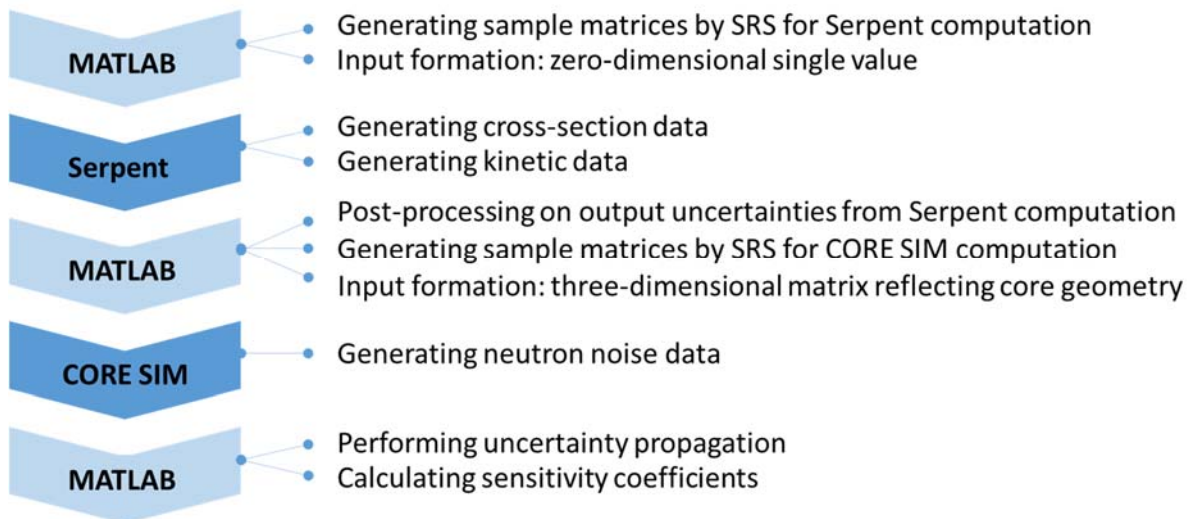


Figure 3: The sequence of codes computation

2.1.7 Neutron Noise Computation using CORE SIM

The core of the CROCUS reactor is approximately cylindrical in shape with a radius of about 65 cm including reflector area and a height of 100 cm. In CORE SIM, the core is modelled with a three-

dimensional mesh of  $43 \times 43 \times 30$  cells, in the x-, y- and z- directions of the core, respectively. The modelled reactor core, at the mid-point of the height, is depicted in Figure 4.

For consistency with a Serpent computation, the core is divided into 4 regions in the radial direction and it is assumed that each region has homogeneous cross-sections as well as other kinetic data. The nuclear data required by CORE SIM are extracted from the Serpent output and assigned to the corresponding nodes of the nodalization scheme automatically by a MATLAB script developed in the course of this work.

Since the water level is lower than the height of fuel elements, around 5 cm of the fuel end-part is exposed to air. Therefore, it is clear that the neutron behavior at the region under the water and above the water must show different trends. The neutron oscillating behavior becomes more remarkable at the higher static-flux region, therefore, the mid-point of the height is chosen as an area of interest because of its high static flux. Additionally, when considering the initial control rod location as fully inserted, the axial neutron flux likely has a bottom skewed shape. In other words, the air exposed region has a relatively lower static flux compared to that of the core region under the water, which results in less influence on a spot having the highest flux. Hence, the fuel end-part above the water level is assumed to have the same kinetic values of that under the water to simplify the core modelling procedure. Nevertheless, to assure the acceptability of this assumption, the neutron noise uncertainty data at the core center region have been compared with and without the air-exposed region. The maximum discrepancy between the two different approaches is 0.15% and 0.23% for the magnitude and the phase, respectively. In other words, the discrepancy is small enough to be neglected and, therefore, it justifies the assumption in this study.

Since CORE SIM performs the calculations in the frequency domain, the resulting neutron noise is a complex quantity. Therefore, the magnitude and the phase of the neutron noise are derived from a post process.

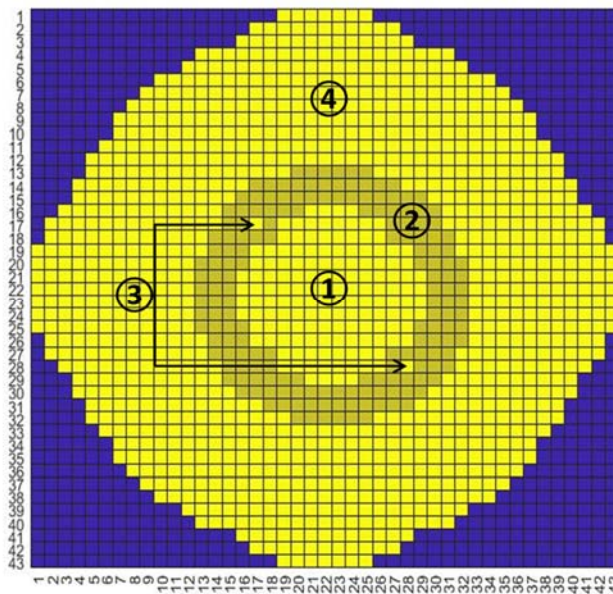


**Figure 4: Modelled reactor core in CORE SIM**

(①: Central zone with  $UO_2$ , ②: Peripheral zone with  $U_{metal}$ , ③: Control rods, ④: Reflector)

## 2.2 Uncertainty Propagation

### 2.2.1 Wilks' Formula

#### 2.2.1.1 Backgrounds

Uncertainty propagation with Wilks' Formula uses the GRS (Gesellschaft für Anlagen und Reaktorsicherheit) methodology, implemented in the code package SUSANA [8]. A Monte-Carlo

method is used to generate  $N$  random samples of the input parameters, taking into account the probability distributions characterizing their uncertainty. These inputs are then processed through  $N$  independent code executions. The outcome is a sample of size  $N$  of the output variables that can be analyzed with non-parametric statistical methods. Such an analysis of the output sample allows a determination of statistical tolerance intervals for the output parameters, with a certain probability content and a certain confidence level. The definition of the confidence interval and the tolerance interval are as below [9].

### Confidence interval

It contains a parameter (like a population mean) with a certain confidence level. For example, if we consider the case of a battery and its lifetime, we might have 95% confidence that mean battery life is from 100 to 110 hours. That means if we repeat the experiment over and over again, 95% of the time the mean battery life will fall into that range.

### Tolerance interval

It covers a specified proportion of the population for a given confidence level. For example, 75% of the time, batteries will fall into the interval 90 to 120 hours, with 95% confidence.

A tolerance interval has a minimum value and a maximum value. These endpoints are called tolerance limits. Tolerance intervals must have a minimum population percentage that we want to cover (e.g. “75% of the population” or “80% of the population”) and a confidence level (commonly, this is set at 95%). The confidence level is the likelihood that a tolerance interval will actually cover the minimum percentage you state. Tolerance intervals can be one-sided (a range where one limit is either negative infinity or positive infinity) or two-sided (a range with a specified minimum and maximum).

The number of necessary code calculations, that is, the size of the output sample, depends on the requested probability content and confidence level of the statistical tolerance limits used in the uncertainty statements of the results. The required minimum number of code runs is given by Wilks’ formula [10]. The equations below describe Wilks’ formula for one-sided (upper) tolerance limit and two-sided tolerance limit, respectively:

$$\sum_{j=0}^{m-1} \binom{N}{j} q^{N-j} (1-q)^j \leq \alpha \quad (6)$$

$$\sum_{i=0}^{r+m-1} \binom{N}{i} (1-q)^i q^{N-i} \leq \alpha \quad (7)$$

where  $\alpha$  is a confidence level,  $q$  is a tolerance limit,  $N$  is a size of samples,  $r$  and  $m$  are the numbers related to the elements in an ordered sample.

Table 4 summarizes the minimum number of code calculations, corresponding to the 1<sup>st</sup> order Wilks’ formula, for two-sided tolerance limits. One-sided tolerance limits require smaller output sample sizes (i.e. code executions).

It is highly recommended to use 95%/95% tolerance limit for combining uncertainties following the U.S.NRC regulatory guide 1.105 [11]. In addition, one of the previous uncertainty studies for best-estimate nuclear system codes, the BEMUSE analysis of the LOFT L2-5 test, indicated that applying Wilks’ formula to the 4<sup>th</sup> or 5<sup>th</sup> order usually produced a more satisfactory tolerance, at the price of some additional code runs [12]. Higher order tolerance limits correspond to values of the ranked output samples away from the maximum and minimum values. They approach progressively with a lower variance, as the order increases, the 5% and 95% quantiles of the true output uncertainty distribution and give a better estimate of these values. The decrease in the variance requires a larger output sample and, therefore a larger number of code executions. Thus, 4<sup>th</sup> order Wilks’ formula for two-sided tolerance limit, which is an optimal option in terms of the computational cost and the level



of conservatism, is considered for the analysis reported hereafter. However, the 1<sup>st</sup> order Wilks' formula is additionally considered for comparison.

**Table 4: Minimum number of calculations for two-sided statistical tolerance limits**

$\beta$ (confidence level)	$\alpha$ (quantile)		
	0.90	0.95	0.99
0.90	38	77	388
0.95	46	93	473
0.99	64	130	662

### 2.2.1.2 Uncertainty Propagation

For the 1<sup>st</sup> order and 4<sup>th</sup> order Wilks' formula for two-sided tolerance limits, 93 times and 260 times of code calculation are required, respectively [13]. In case of the 1<sup>st</sup> order Wilks' formula, the largest and the lowest values among 93 calculation results credit the uncertainty propagation result to satisfy the 95%-95% criterion. Similarly, the relevant values are the 4<sup>th</sup> largest and the 4<sup>th</sup> smallest values for the case of 4<sup>th</sup> order Wilks' formula.

## 2.2.2 Monte-Carlo approach

### 2.2.2.1 Background

The Monte-Carlo method has been selected as a comparison against the approach based on Wilks' formula. This method is well-known as an alternative to the more cumbersome perturbation methods used extensively over the world for neutronic calculations. The method takes advantage of the large computational power available nowadays [14]. For the comparison with the uncertainty quantification results from Wilks' formula, 95%-5% percentiles are calculated for the probability distributions of the output uncertainty with this method.

The advantages of the Monte-Carlo approach can be boiled down to two items. First, the result of the uncertainty propagation shows more realistic values with a large number of sample runs. Especially, this can be a competitive edge when compared to the results from Wilks' formula, which cover the required probability (95% to 5%) with a certain confidence level for any case. Another point is that this approach can yield the full PDF of the value of interest. Once a PDF is defined, we can expect that whichever sample runs we make, the result will have the same distribution as we obtained earlier. In other words, we can be always safe when making the parametric assumptions about the sampling distribution, regardless of the sample size [15].

### 2.2.2.2 Surrogate Modelling

Numerical studies including reliability analysis or sensitivity analysis on physical models tend to require a higher number of runs in order to catch the proper tendency on model response due to the values of the input parameters. However, these techniques require a large number of model evaluations, which are often unacceptable for time expensive computer codes. The solution consists in substituting the physical model  $M$  with a mathematical approximation  $\hat{M}$  built from a set of data samples. Such an approximation is referred to as a surrogate model or a meta-model. A software package DACE (Design and Analysis of Computer Experiments) is developed, which is a MATLAB toolbox for working with kriging approximations to computer models and makes it possible to predict the output from a computer model at untried inputs [16]. The kriging approximation is an optimal interpolation based on a regression against observed values of surrounding data points, weighted according to spatial covariance values. The kriging interpolation model effectively represents the response as the sum of a realization of a regression model and the correlation model. The further explanations on each model are as below [17].



**Regression model**

The regression model represents the general trend of the samples and is modelled with a low order polynomial. The importance of the regression model varies with the density of the samples. If samples are close, then the effect of correlation from the samples will dominate the appearance of the model. The better the regression model fits the data, the less the correlation model is exploited to explain global behavior. Three options of zero order, first order and second order polynomial are provided by the DACE package.

**Correlation model**

The correlation model parameters are closely interlaced with the regression parameters. The effect of the correlation model is to explain deviations from the general trend. This model can be one of these functions: exponential, general exponential, Gaussian, linear, spherical and cubic spline. If the underlying phenomenon is continuously differentiable, the correlation function will likely show a parabolic behavior near the origin, which means that choosing the Gaussian or the cubic spline function would be recommended.

In this study, considering the complexity underlying the neutron noise behavior, the second order polynomial and the Gaussian function are selected for further analysis as a regression model and a correlation model, respectively. The obtained mean squared error (MSE) of the predictor are shown as 7E-4 for the magnitude of the noise and 1E-4 for the phase of the noise, where 20,000 cases are predicted from 500 cases.

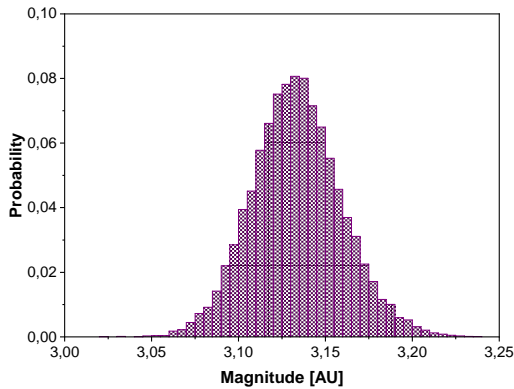
**2.2.2.3 Empirical Probability Density Function**

After 500 times of actual code execution, the size of sample matrices is increased to 20,000 by the aid of surrogate modelling.

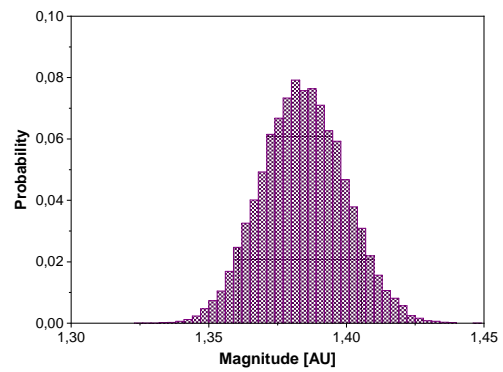
As can be seen in Figure 5, a histogram for the whole population is made by MATLAB. To confirm the normality of the output results, a series of normality test is performed with the Shapiro-Wilk test and the obtained normality p-value is summarized in Table 5. Since all the p-values are large enough (typically > 0.05), the hypothesis of normality for the outputs cannot be rejected at a significance level of 5% and thus it can be considered reasonable.

**Table 5: Shapiro-Wilks test for normality p-value for neutron noise data**

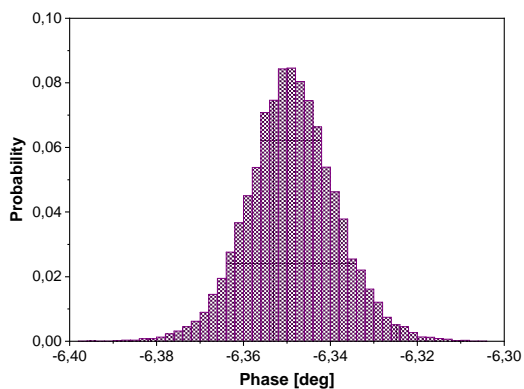
Parameter	p-value
Magnitude of fast neutron noise	0.0698
Magnitude of thermal neutron noise	0.1005
Phase of fast neutron noise	0.6492
Phase of thermal neutron noise	0.8818



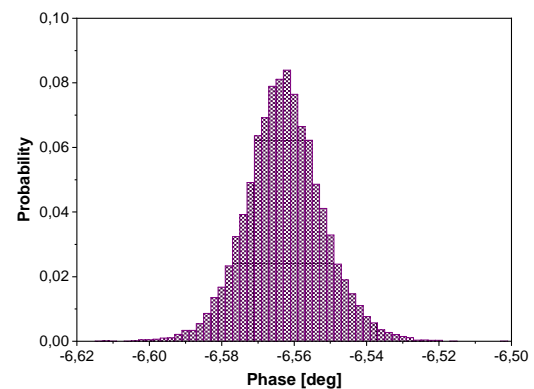
a. Magnitude of fast neutron noise



b. Magnitude of thermal neutron noise



c. Phase of fast neutron noise



d. Phase of thermal neutron noise

**Figure 5: Probability density function for neutron noise data**

#### 2.2.2.4 Uncertainty Propagation

After increasing the total number of sample sets by surrogate modelling, the 95% upper limit and lower limit values are obtained by a direct counting of the neutron noise data at the 95% and 5% population level.

#### 2.2.3 Discussions

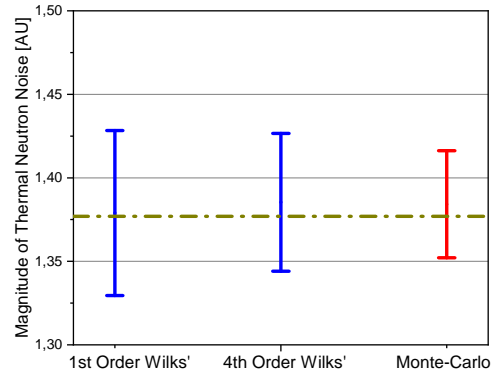
Figure 6 shows the comparison of the results from the Wilks' formula-based methodology and Monte-Carlo approach. The nominal value is obtained from the combination of the mean values of the parameters reported in Table 2.

Above all, the 1<sup>st</sup> order and the 4<sup>th</sup> order of Wilks' formula show wider, more conservative ranges than the Monte-Carlo approach. When the result from 1<sup>st</sup> order Wilks' formula is compared to that from 4<sup>th</sup> order Wilks' formula, the 1<sup>st</sup> order Wilks' formula tends to give more conservative range, because of the less accurate estimate of the percentiles. Since the tolerance limit is an approximation to the true population, there is an inherent conservatism in the typical prediction as in the formulation above. In case of  $N = 93$ , which is the minimum size of samples for 1<sup>st</sup> order Wilks' formula, there is a tendency to strongly over-estimate the 95<sup>th</sup> quantile of the population and under-estimate the 5<sup>th</sup> quantile of the population. However, the conservatism diminishes as the size of the sample increases. Therefore, the result from 4<sup>th</sup> order Wilks' formula shows a smaller uncertainty range, which is more realistic outcome than the result from 1<sup>st</sup> order Wilks' formula.

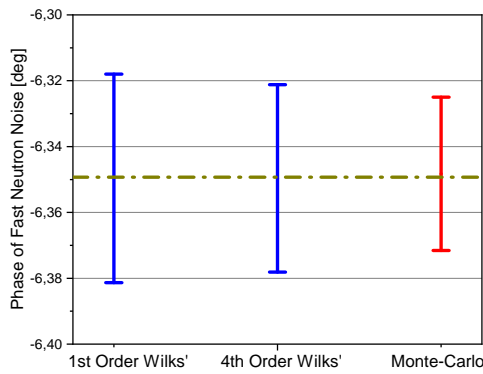
- Upper/Lower bound for 95% tolerance limit + 95% confidence level
- Upper/Lower bound for 95% tolerance limit
- - - Nominal value



a. Magnitude of fast neutron noise



b. Magnitude of thermal neutron noise



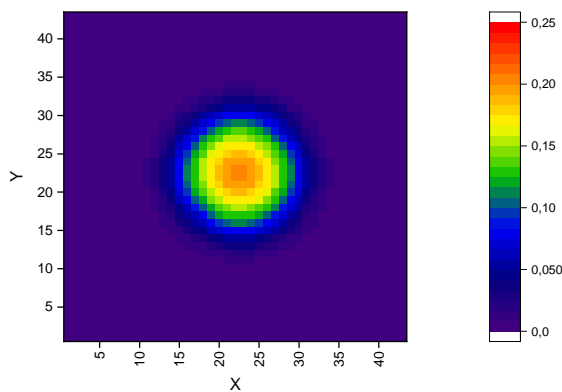
c. Phase of fast neutron noise



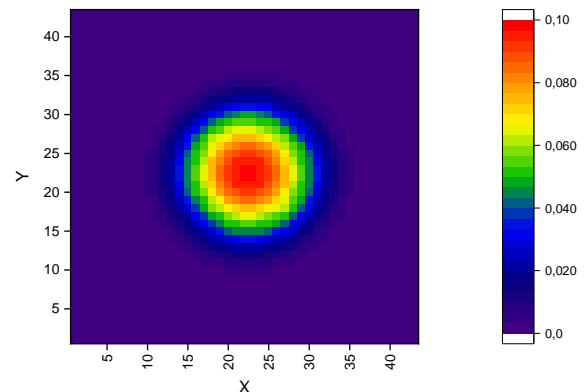
d. Phase of thermal neutron noise

**Figure 6: Uncertainty range estimated with different approaches**

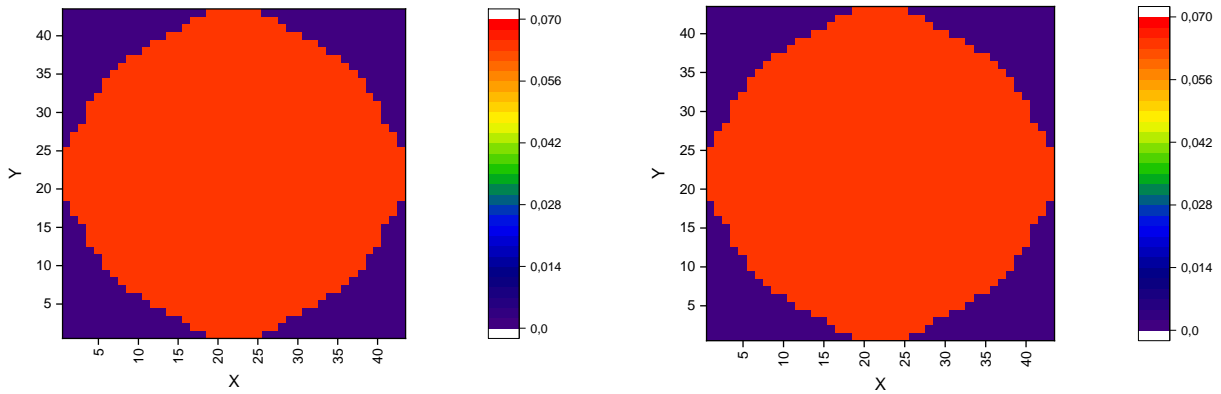
### 2.2.4 Space dependency of the neutron noise uncertainty



a. Magnitude of fast neutron noise



b. Magnitude of thermal neutron noise

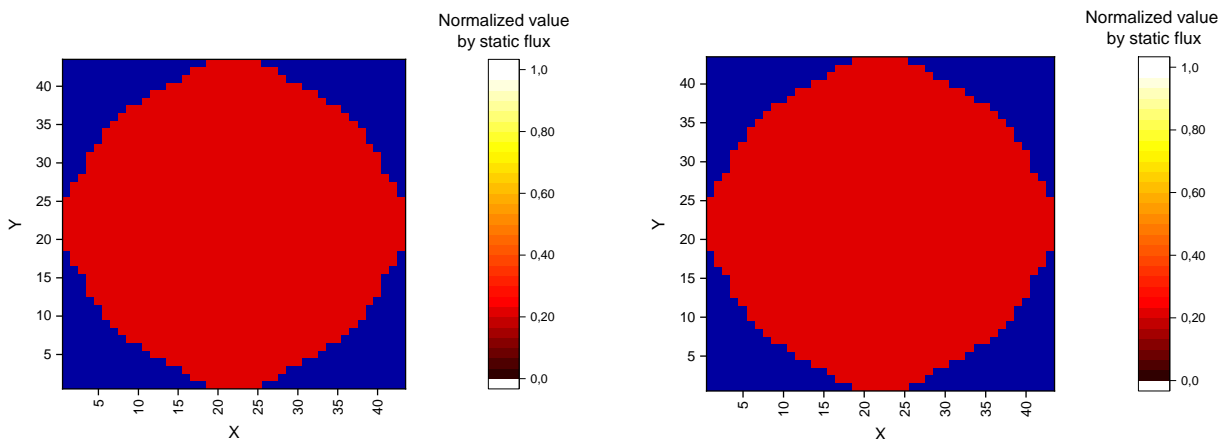


c. Phase of fast neutron noise

d. Phase of thermal neutron noise

**Figure 7: The trends on the range of the noise uncertainty range in radial direction of the core (axial level  $k = 15$ )**

As an example of the spatial distribution of the output uncertainties, the plane at mid-elevation of the reactor core is taken. Figure 7 depicts the result for both magnitude and phase. As it can be seen in these graphs, the uncertainty range of the magnitude has a spatial dependency for both the fast and the thermal neutron noise, while the uncertainty in the phase is approximately constant. In graphs *a* and *b*, the values become larger as the location gets closer to the center of the core. For a better understanding, these uncertainty range data regarding the magnitude of neutron noise are normalized by the static neutron flux at the corresponding node and are shown in Figure 8. Here the normalized uncertainties show a uniform value throughout the core region. This implies that the range of the neutron noise uncertainty is highly correlated with the static flux. In addition, the uncertainty range of the phase shows no strong spatial dependency as shown in graphs *c* and *d*. These results are expected because all the fuel rods in the central part of the core are perturbed at the same time and in the same manner. Moreover, since the reactor core is relatively small, the point-kinetic component of the system response to perturbations is overwhelming. The amplitude of the neutron noise thus follows the static flux, whereas the phase of the neutron noise is spatially homogeneous.



a. Magnitude of fast neutron noise

b. Magnitude of thermal neutron noise

**Figure 8: Normalized noise uncertainty by the static neutron flux**

### 2.3 Sensitivity Analysis

There are three approaches available to measure the importance of input variables: regression-based coefficients, correlation-based coefficients and variance-based coefficients. Among these,

correlation-based coefficients and variance-based coefficients are selected for further sensitivity analysis.

The main physical processes underlying neutron flux oscillations are generally nonlinear and non-monotonic, and there are important interactions between the parameters that influence them. Therefore, variance-based analysis which is generally based on the decomposition of the output variance, is regarded as a proper approach for this study. Nevertheless, the correlation-based approach is considered here as well to acquire a better understanding of the overall sensitivity analysis results and applicability to neutron noise studies.

### 2.3.1 Correlation-based coefficients

#### 2.3.1.1 Backgrounds

The use of correlation-based coefficient, as well as regression-based coefficients are traditional approaches extensively used to assess the strength of the association between two factors due to their relatively simple statistical theories [18].

The Spearman's rank correlation coefficient ( $r_s$ ) is a non-parametric measure of rank correlation. This coefficient measures the strength and the direction of association between two ranked variables and can be computed following the equation below:

$$r_s = \frac{cov(r_{g_X}, r_{g_Y})}{\sigma_{r_{g_X}} \sigma_{r_{g_Y}}} \quad (8)$$

where  $\sigma_{r_{g_X}}$  and  $\sigma_{r_{g_Y}}$  are the standard deviations of the rank variables and  $cov(r_{g_X}, r_{g_Y})$  is the covariance of the rank variables.

The correlation-based coefficient, however, has as a disadvantage that it can draw only a limited conclusion in the case of general nonlinear and non-monotonic models. In addition,  $r_s$  cannot be used to say anything about a cause and effect relationship. We could only conclude that the input parameter and output value are related by examining the value of  $r_s$ . However, the same value of  $r_s$  does not tell us if the input parameter influences the output value or the other way around. Then, the correlation-based coefficient should not be the primary tool used to study causation, because of the problem with the influence of third variables.

In this regard, calculating the Spearman's Partial Correlation Coefficient (PCC) can be helpful to check the direct effect of each input parameter on the output value. The Spearman's PCC provides a measure of strength of the correlation between the individual input parameter and output value when the effect of all of the other parameters are removed.

In the case of one explained output value  $Y$  and two explicative input parameters  $X_1$  and  $X_2$ , the PCC can be estimated as follows:

$$r_{Y, X_1 | X_2} = \frac{r_{Y, X_1} - r_{Y, X_2} r_{X_1, X_2}}{(1 - r_{Y, X_2}^2)^{\frac{1}{2}} (1 - r_{X_1, X_2}^2)^{\frac{1}{2}}} \quad (9)$$

The recursive formula in the general case is provided in the following equation:

$$r_{Y, X_j | X_{\sim j}} = \frac{r_{Y, X_j | X_{1,2,\dots,j-1,j+1,\dots,N-1}} - r_{Y, X_N | X_{1,2,\dots,N-1}} r_{X_j, X_N | X_{1,2,\dots,j-1,j+1,\dots,N-1}}}{(1 - r_{Y, X_N | X_{1,2,\dots,N-1}}^2)^{\frac{1}{2}} (1 - r_{X_j, X_N | X_{1,2,\dots,j-1,j+1,\dots,N-1}}^2)^{\frac{1}{2}}} \quad (10)$$

where  $X_{\sim j} = X_{1,2,\dots,j-1,j+1,\dots,N}$ .

However, apart from its applicability for checking the individual effect on output value, PCCs do not yield any relevant information regarding the relative importance of the explicative variables. In other words, PCCs will be used in this study only to check the degree of the collaboration between the parameters, not to find the most affecting parameters on neutron noise which corresponds to the original purpose of the sensitivity analysis.



### 2.3.1.2 Results

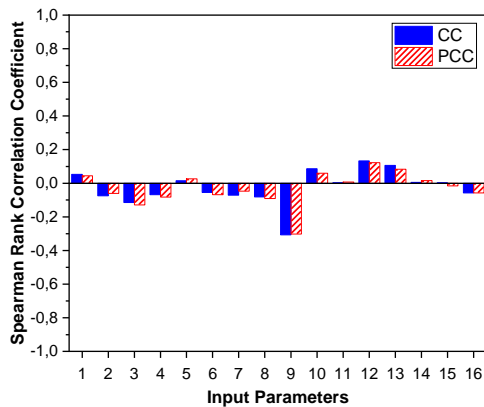
Figure 9 illustrates the calculated rank Correlation Coefficients (CC) and Partial Correlation Coefficients (PCC) estimated for 16 out of the 26 input parameters listed in in Table 2. Since the other 10 parameters are dependent on the selected 16 parameters according to the correlations described in the Table 2, their sensitivity coefficients are directly correlated to those of selected parameters. Therefore, the 16 main parameters leading the phenomenon are regarded as having a higher priority and only considered for further analysis.

Following the guidelines regarding the interpretation of the CCs [19], a coefficient ranging between -0.3 and 0.3 is translated as ‘negligible correlation’. Therefore, we can say that no input parameter shows any remarkable correlation with the phase of neutron noise. The same goes for the general trend of the magnitude of neutron noise except for the 9<sup>th</sup> input parameter, which stands for ‘fuel rod outer diameter of the cladding’, in reality the diameter of the fuel rod.

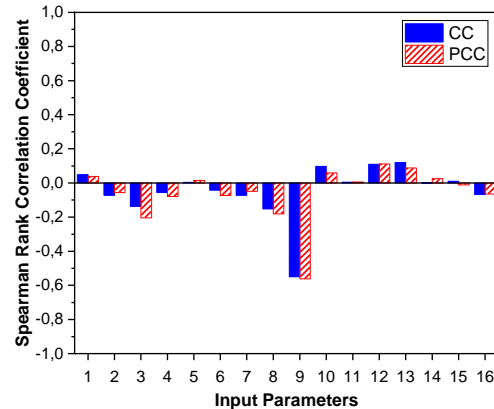
In terms of the PCCs, the results can be translated as follows:

- 1) If PCC is larger than CC, the input parameter ( $X_j$ ) has a direct effect to the output result ( $Y$ ). However, the contribution of  $X_j$  is screened because of its relatively small initial uncertainty range or small weighting factor applied to this parameter compared to other parameters ( $X_k, j \neq k$ ). That is to say, the collaboration with other parameters works towards decreasing the amount of effect on  $Y$ .
- 2) If PCC is smaller than CC,  $X_j$  increases its influence by the cooperation with other parameters. However, as depicted in Figure 9, there is no remarkable difference between the results from CC and PCC. Therefore, it is concluded that correlation-based approach expects no strong collaboration between the input parameters.

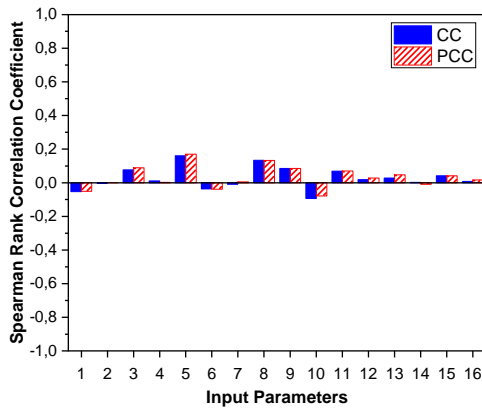
Meanwhile, despite this result, it is hard to conclude that the input parameters showing negligible correlation here have actually no effect on the output data. Since the monotonic relationship between the input and the output data is the main concern of the Spearman’s rank correlation coefficient, there is a possibility that the real correlation is concealed due to its non-monotonic relationship. Therefore, we need to check the true correlation through the additional variance-based approaches.



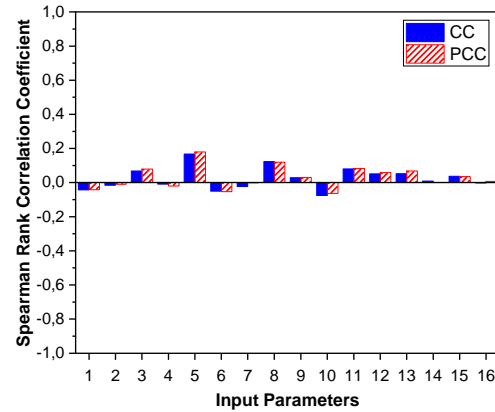
a. Magnitude of fast neutron noise



b. Magnitude of thermal neutron noise



c. Phase of fast neutron noise



d. Phase of thermal neutron noise

1	Water level	9	Fuel rod outer diameter of cladding (UO <sub>2</sub> )
2	Initial pool temperature	10	Fuel rod outer diameter (U <sub>metal</sub> )
3	Fuel density (UO <sub>2</sub> )	11	Fuel rod outer diameter of cladding (U <sub>metal</sub> )
4	Fuel density (U <sub>metal</sub> )	12	Cladding thickness (UO <sub>2</sub> )
5	Enrichment (UO <sub>2</sub> )	13	Cladding thickness (U <sub>metal</sub> )
6	Enrichment (U <sub>metal</sub> )	14	Square pitch (UO <sub>2</sub> )
7	Active fuel length	15	Square pitch (U <sub>metal</sub> )
8	Fuel rod outer diameter (UO <sub>2</sub> )	16	Initial position of control rod

Figure 9: Spearman rank and partial correlation coefficients for neutron noise data

### 2.3.2 Variance-based coefficient

#### 2.3.2.1 Background

In many variance-based sensitivity analysis methods, the variance is used as an indicator of the importance of an input variable. Among many methods for analysing the decomposition of variance as a sensitivity measure, the method developed by Sobol is one of the most well-established and widely used [20]. Following Sobol's method, we can obtain the first order sensitivity index ( $S_i$ ) and the total sensitivity index ( $S_{T_i}$ ). The first order index represents the main effect contribution of each input parameter to the variance of the output. Meanwhile, the total sensitivity index measures the contribution to the output variance of input parameter including all the interactions with other input variables. These indices can be obtained following the equations below:

$$S_i = \frac{V(E(Y|X_i))}{V(Y)} \quad (11)$$

$$S_{T_i} = \frac{E(V(Y|X_{\sim i}))}{V(Y)} = 1 - \frac{V(E(Y|X_{\sim i}))}{V(Y)} \quad (12)$$

where  $X_i$  is  $i^{th}$  input parameter,  $Y$  is a model output and  $X_{\sim i}$  means  $N \times (k - 1)$  matrix of all factors but  $X_i$ , with  $N$  the sample size and  $k$  the number of samples. The detailed information on calculating Sobol's sensitivity indices using the decomposition of variance can be found in other references [21].

To get the precise estimates on the sensitivity indices, this approach is costly in terms of the number of model cells. In common practice, the value of  $10^4$  model evaluations can be required to estimate

the Sobol's index with a statistical error of 10% [22]. Therefore, there have been many attempts to find more efficient ways to compute the first order and total sensitivity indices. Among them, Jansen's formula is considered as the best way especially for estimating the total effect [23]. The improved estimator for both first order sensitivity index ( $S_i$ ) and total sensitivity index ( $S_{T_i}$ ) is given by the formulas described below [24]:

$$V(E(Y|X_i)) = V(Y) - \frac{1}{2N} \sum_{j=1}^N (f(B)_j - f(A_B^{(i)})_j)^2 \quad (13)$$

$$E(V(Y|X_{\sim i})) = \frac{1}{2N} \sum_{j=1}^N (f(A)_j - f(A_B^{(i)})_j)^2 \quad (14)$$

where  $A_B^{(i)}$  is a matrix, column  $i$  comes from matrix  $B$  and all other  $k - 1$  columns come from matrix  $A$ .

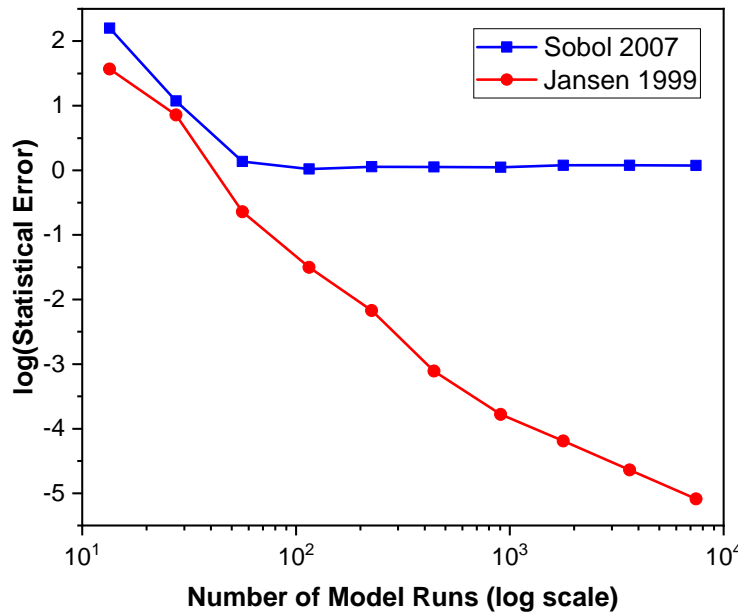


**Figure 10: Comparison of statistical error from 'Jansen 1999' and 'Sobol 2007' at increasing number of model runs**

Moreover, Jansen's formula requires  $N \times (k + 2)$  model evaluations rather than  $N \times (2k + 1)$  from the original Sobol's formula, resulting in improved computational costs. In addition, it was proven that Jansen's approach has even less statistical error compared to Sobol's approach, as shown in Figure 10. When the sampling size becomes larger, the statistical error of Jansen's approach decreases dramatically while that of Sobol's approach becomes saturated at some point and maintains this value as depicted in Figure 10 [25].

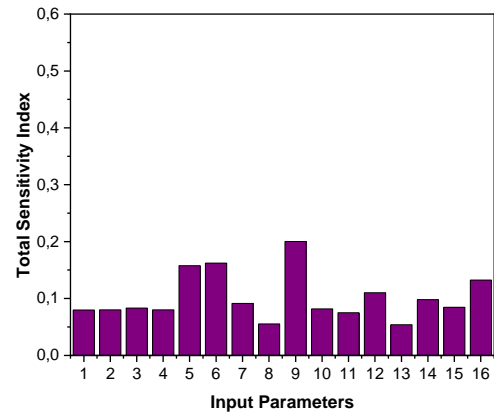
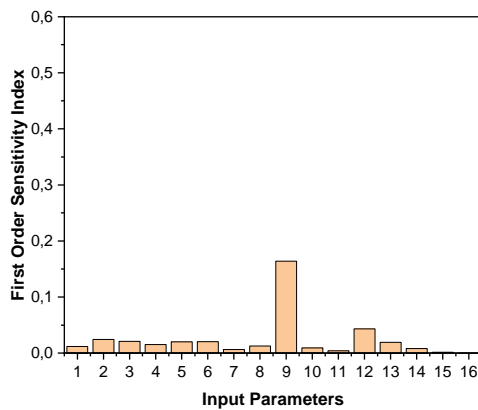
### 2.3.2.2 Results

Figure 11 presents the first order and the total sensitivity indices for the neutron noise data. Following the previous studies regarding variance-based sensitivity analysis, the parameters with sensitivity indices larger than 0.1 can be regarded as 'highly sensitive' and the indices between 0.01 and 0.1 can be classified into 'sensitive' [26].

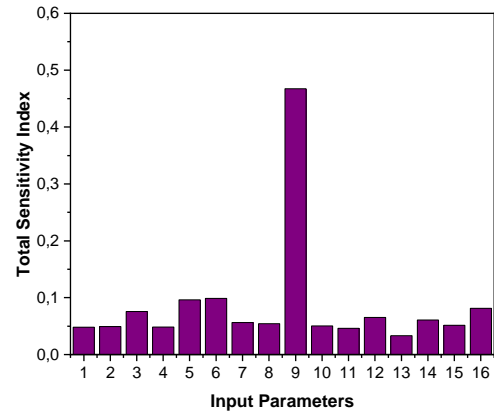
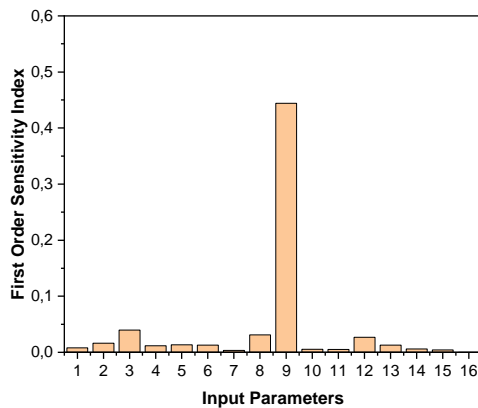
In this context, when we glance over the graphs for the first order sensitivity index, the 9<sup>th</sup> input parameter has the dominant effect on the magnitude of neutron noise, also seen with the correlation-based sensitivity, which shows the consistency of both sensitivity analyses. However, there is no

‘highly sensitive’ input parameter which is affecting the phase of neutron noise, as was also the case of the Spearman’s coefficients.

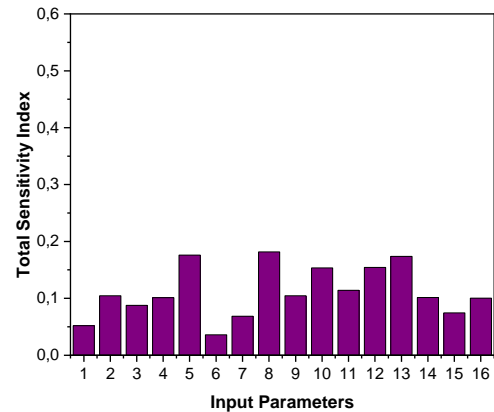
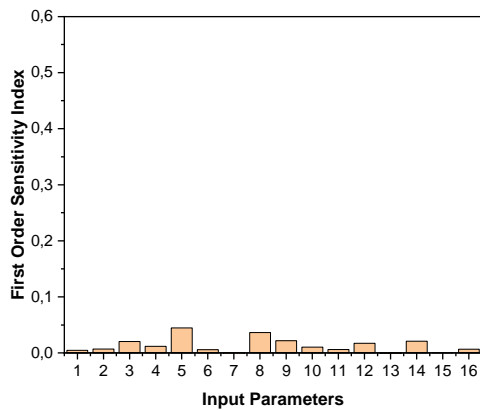
For the total sensitivity indices, all the values are larger than the first order sensitivity indices, which is a natural tendency because the total index represents the effect of all the group of variables that contain the parameter of interest. In case of the magnitude of neutron noise, the 9<sup>th</sup> parameter still remains as the most influential parameter and it is followed by the enrichment of the fuel. Meanwhile, there is no clear dominant parameter on the phase of the neutron noise, even though all the total sensitivity indices become larger than the first order indices. Hence, it can be concluded that each input parameter is affecting the phase of the neutron noise not only by itself, but also by the collaboration with other parameters and the influence of each parameter is about the same.



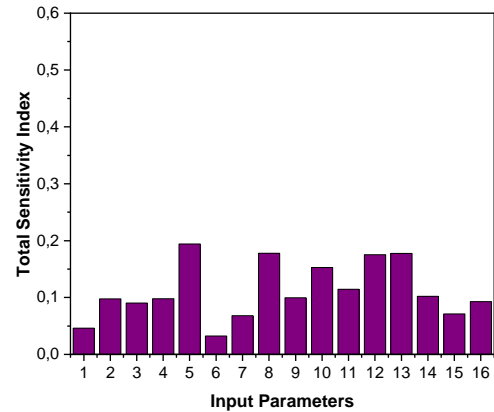
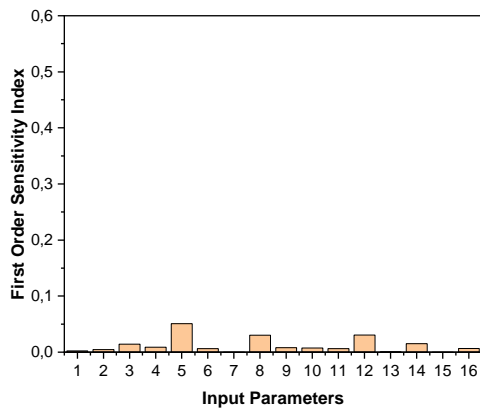
a. Magnitude of fast neutron noise



b. Magnitude of thermal neutron noise



c. Phase of fast neutron noise



d. Phase of thermal neutron noise

1	Water level	9	Fuel rod outer diameter of cladding (UO <sub>2</sub> )
2	Initial pool temperature	10	Fuel rod outer diameter (U <sub>metal</sub> )
3	Fuel density (UO <sub>2</sub> )	11	Fuel rod outer diameter of cladding (U <sub>metal</sub> )
4	Fuel density (U <sub>metal</sub> )	12	Cladding thickness (UO <sub>2</sub> )
5	Enrichment (UO <sub>2</sub> )	13	Cladding thickness (U <sub>metal</sub> )
6	Enrichment (U <sub>metal</sub> )	14	Square pitch (UO <sub>2</sub> )
7	Active fuel length	15	Square pitch (U <sub>metal</sub> )
8	Fuel rod outer diameter (UO <sub>2</sub> )	16	Initial position of control rod

Figure 11: Variance-based sensitivity indices for neutron noise data; first order sensitivity index (left) and total sensitivity index (right)

### 2.3.3 Discussions

As summarized in 2.3.1.2 and 2.3.2.2, the UO<sub>2</sub> fuel rod outer diameter (variable No. 9) shows the maximum effect on the magnitude of the neutron noise. Since this parameter directly affects the area occupied by the fuel inside of the core, it contributes to the changes on moderator-to-fuel ratio as a result. In other words, the increased fuel rod outer diameter results in the decrease of the resonance escape probability and the increase of the thermal utilization factor. Therefore, it changes the

effective neutron multiplication factor ( $k_{eff}$ ), which affects the static and dynamic behaviour of the neutron flux and ultimately the neutron noise.

It is also an interesting point that only the outer diameter of  $UO_2$  has a remarkable effect on neutron noise whereas the outer diameter of  $U_{metal}$  has no strong effect. It is inferred that this difference stems from the followings: the differences on initial uncertainties and the total number of fuel rods. The outer diameter of  $UO_2$  has an uncertainty range which is two times bigger than that of  $U_{metal}$ . Plus, there are 336 rods for  $UO_2$  fuels and 176 rods for  $U_{metal}$  fuels. Therefore, the uniform change of cladding thickness of  $UO_2$  fuels results in a bigger decline of the moderator-to-fuel ratio than by the change of  $U_{metal}$  fuels. In addition, the perturbation introduced in the system and inducing the neutron noise is directly associated with the  $UO_2$  fuel rods.

When the results from two different approaches are compared to each other, we can summarize that the first order sensitivity index derives the bigger correlation in comparison with the correlation-based approach. Moreover, the total sensitivity index makes it possible to predict the hidden collaboration between the parameters, which is invisible with the correlation-based approach. Therefore, in terms of the suitability for the analysis of the neutron noise behavior, it can be concluded that the variance-based approach is appropriate.

### 3 Analysis of Nuclear Oscillatory Phenomena using Spectral / Frequency Decomposition

The text in this section describes the methodology developed by Stefan Walser during his PhD work at the Chair of Nuclear Technology of the Technical University of Munich (TUM) directed by Prof. Rafael Macián [27]. This methodology is planned to be used in the context of the project CORTEX for time-dependent analyses of neutronic oscillations when the required data is available from simulations carried out in some of the work packages.

#### 3.1 Basis of the Methodology

The methodology is based on the application of the Fast Fourier Transform (FFT) to the analysis in frequency and phase of reactor time varying variables. If the variables are selected such that they characterize the neutronic behavior and any physical reactivity mechanism, then correlations can be found that can shed light on the influence of the reactivity feedback on the reactor neutronic variables, e.g. the neutron flux.

The main advantage of this methodology is the possibility to apply it to two- or three-dimensional geometries in scales that can span core regions, fuel assemblies or individual fuel rods. The scale depends on the resolution of the time dependent calculations in both time and space.

The spectral analysis is capable of identifying frequencies and associated amplitudes in the time values of the variables processed. Thus, an infinite sum of sinusoidal functions can represent a periodical time-function at equally spaced frequencies with an interval  $1/T$  in a Fourier series expansion, in which  $T$  is the period of the function. For this reason, the Fourier transform is used to decompose time series signals into their frequency components, with each one of them consisting of an amplitude and a phase. The inverse Fourier transformation reconstructs the information from the frequency-domain back into the time domain of the original variable.

The Discrete Fourier Transform (DFT), which transforms a discrete time domain signal into a discrete frequency domain representation, is defined as:

$$X[k] = \sum_{n=0}^{N-1} x[n] \cdot e^{-j2\pi k \frac{n}{N}} \quad (15)$$

with  $X$ : the frequency domain representation of the signal time-series signal  $x$ , the formula yields a complex number  $X[k]$  for every  $k$ .

$k$ : the  $k$ -th frequency component;  $k = 0, 1, \dots, N - 1$ ,  
 $N$ : the total number of samples of the signal variable  $x$ ,  
 $x$ : the time series signal variable;  $n = 0, 1, \dots, N - 1$ ,  
 $n$ : the  $n$ -th sample (in the time domain), and  
 $j$ : the imaginary unit.

The  $k$ -th basis function is defined as:

$$e_k[n] = e^{-j2\pi k \frac{n}{N}} \quad (16)$$

The phase angle of the complex number is described as:

$$\varphi[n] = \frac{k \cdot n}{N} 2\pi \quad (17)$$

The formula for transforming a signal in the frequency-domain back into the time domain, the inverse transform, is calculated as a summation over all the frequency components  $k$ :

$$x[n] = \frac{1}{N} \sum_{k=0}^{N-1} X[k] e^{j2\pi k \frac{n}{N}} \quad (18)$$

The FFT is a version of the DFT which uses special algorithms to allow for a much faster calculation and is available as an implemented function in many computational software packages and computer languages. In particular, for this work, the computational system MATLAB will be used and the functions  $Y = \text{fft}(X)$  and  $Y = \text{ifft}(X)$  are used to calculate the forward and inverse FFT given vector of  $N$  values (time series) of the variable  $x$ .

### 3.2 The Application of the FFT on the Global Parameter Reactor Power

In this section a special case is used to illustrate the application of the methodology to global reactor parameters. The work was reported in the PhD thesis of Stefan Walser [27]. The transient analyzed is a feedwater reduction event in a BWR with full thermal-hydraulic three-dimensional coupled feedback. It was simulated with the TRACE-PARCS coupled code system and represents a real event which took place in one of the Swedish BWR Plants. In [27] the reader can find a more detailed description of the simulation, its accuracy and the models used for it.

The signal variables in the analysis are physical quantities describing the behavior of the reactor. They can also be related to changes in reactor configuration, such as movement of reflectors, control rods or fuel assemblies. The changes of the variables as a function of time constitute the time-series which can be processed with the FFT algorithm in a global or local scale. The ultimate goal is to use the spectral analysis of the different feed-back variables and that of the output signal of interest to find amplitude and phase correlations that can shed light on the complex interaction mechanisms.

Changes in the mean values of the variables are of no of interest in this analysis, but solely the oscillating component of the signal is of peculiar interest in the FFT output. Therefore, the offset that represents the average value is eliminated from the signal and its variation with time, shown as a slope in the complete signal. The slope can also vary with time, but more slowly than the oscillatory component of the signal. This is carried out by subtracting the offset value from linear function fitted to the slope of the input signal as presented in Figure 12 and Figure 14.

The processed input signal without its offset and slope, which describes solely the oscillating part of the signal, is shown in Figure 15. The FFT is applied to this signal and its spectral components are shown in Figure 16, while Figure 13 describes the result after applying FFT on the original reactor power signal. Significant amplitude peaks are obvious at a frequency of about  $f = 0.5$  Hz.

This is in accordance with the definition of the frequency where the number of cycles and the time interval are read from Figure 15:

$$f = \frac{\text{number of cycles}}{\text{time interval}} = \frac{8 \text{ oscillations}}{16.4 \text{ seconds}} = 0.488 \text{ Hz} \quad (19)$$

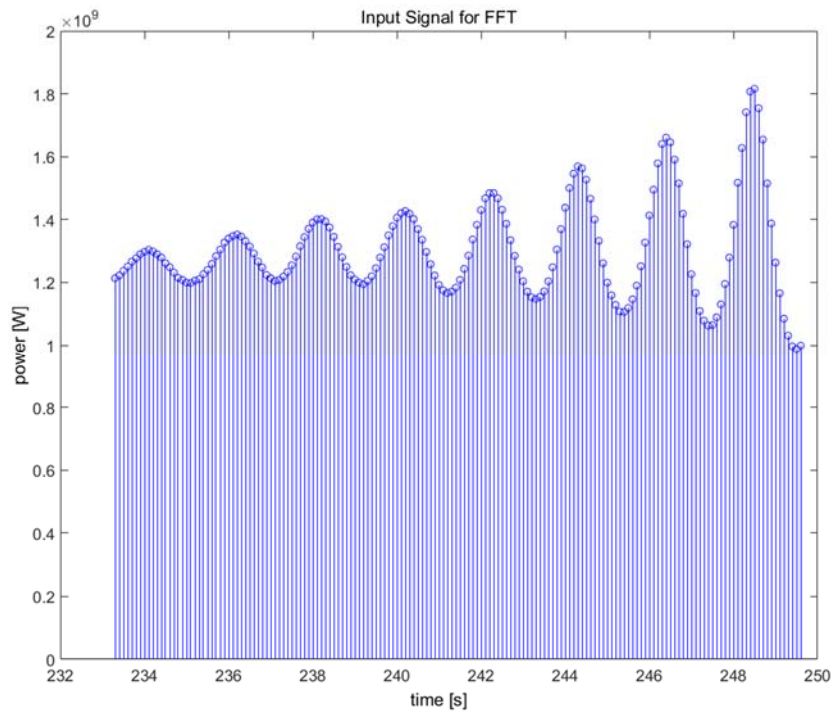


**Figure 12: Section of a feedwater transient in a BWR with an unbounded power oscillation: Total Reactor Power**

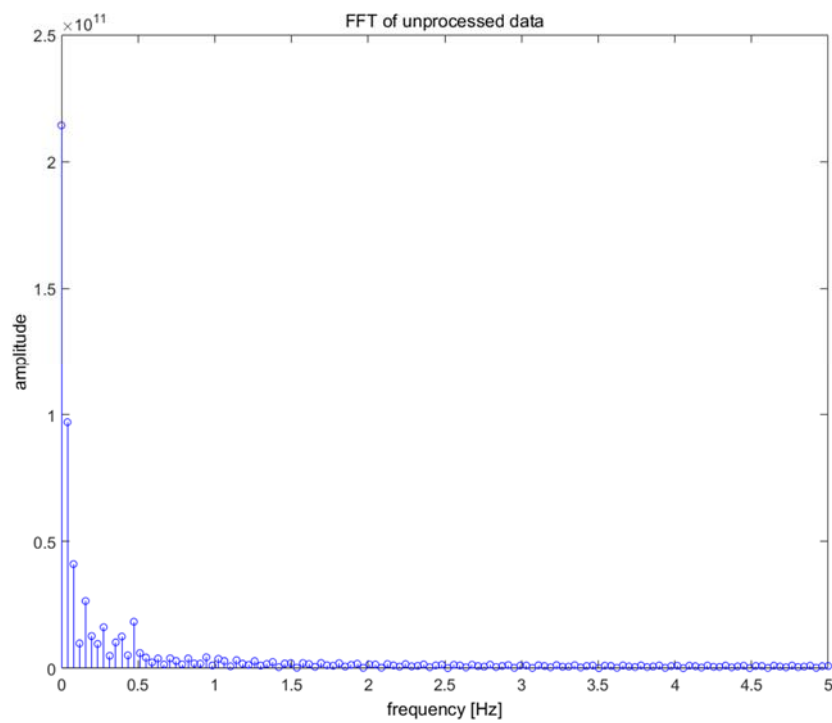


**Figure 13: Spectral analysis of the power signal in Figure 12. The signal is characterized by a high amplitude with a frequency of  $f = 0$  Hz resulting from the offset, that is, the mean value of the input signal.**

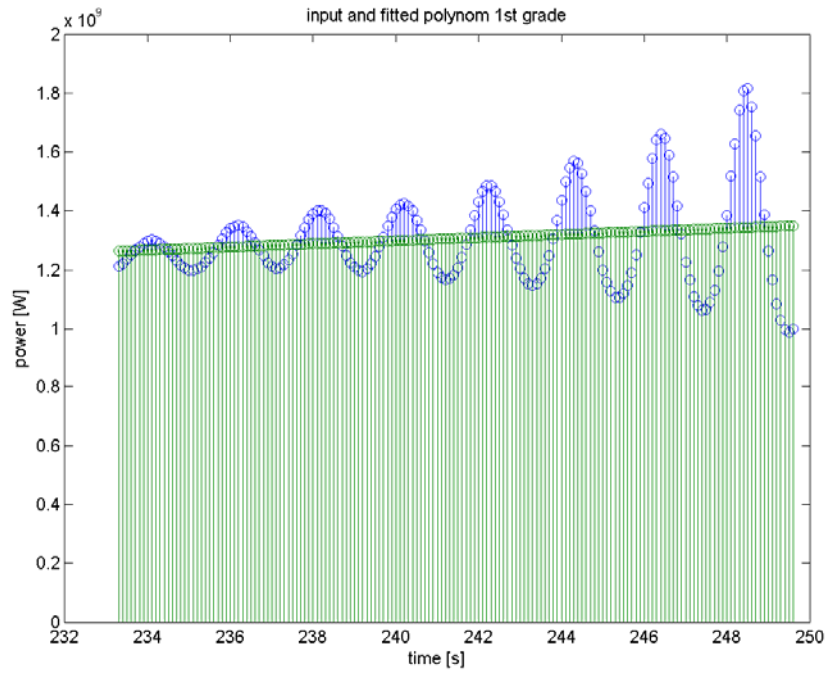


**Figure 14: Power signal and fitted polynomial of 1<sup>st</sup> grade (linear fitting): the average value of the signal is then represented by the green line, which, because the power rises steadily with time has a positive slope with time.**

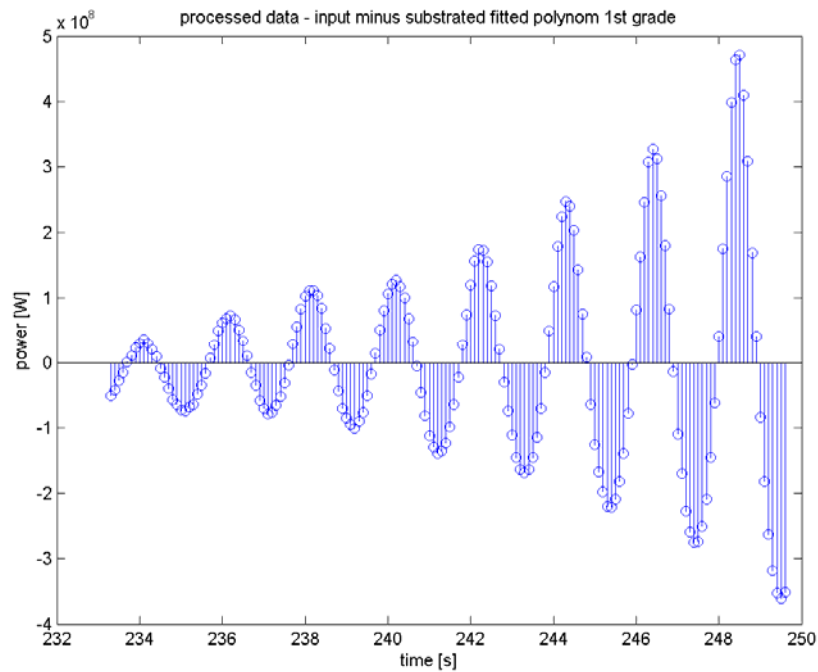


**Figure 15: Oscillatory component of the power signal after the linearly growing average value is subtracted. The signal is then ready to be spectrally processed.**

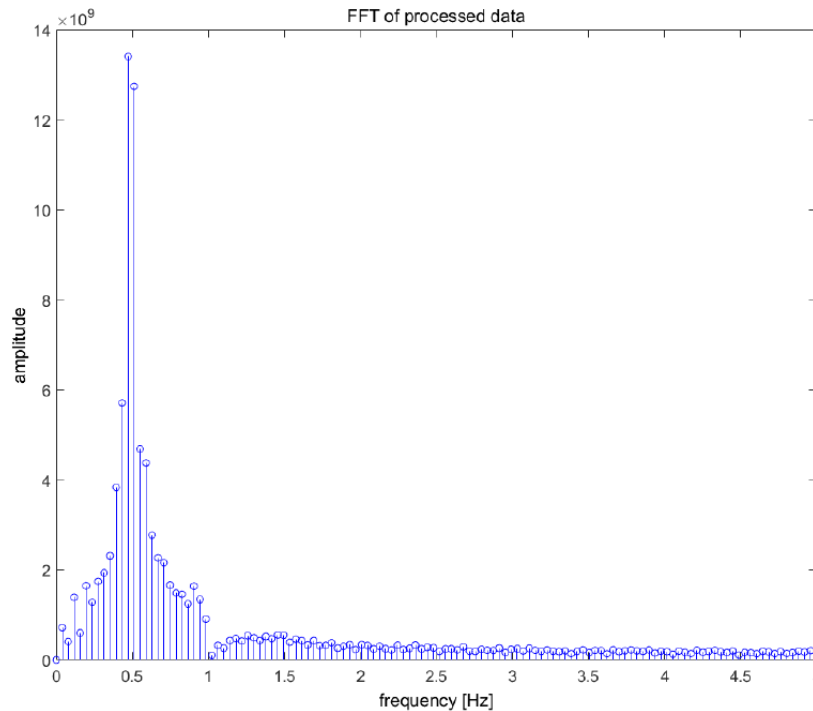


**Figure 16: Spectral analysis of the oscillation signal**

In this example, no other reactor variables, such as average core pressure, density or temperature have been shown, but a similar set of plots can be obtained, and a comparison can be made mostly on the phase values. Based on the analysis, insights can be obtained into the influence of these variables on the power (or average neutron flux). In this particular scenario, given the important feedback mechanisms involved, global parameters do not show a detailed reactor behavior, since the interaction of the moderator density, rod temperatures and along-the-rod pressure variations are of a local quality and they influence the oscillatory behavior at the level of fuel assemblies. Such oscillations are propagated to the entire core and result in the power profile shown in Figure 12. Other types of transients may be more suitable to only global analysis. In any case, the methodology work in the same manner.

### 3.3 The Application of the FFT to Local Physical Parameters

The methodology was also applied in [27] to the local analysis of neutron flux (and power) oscillations in a three-dimensional, time-dependent manner at the fuel assembly (flow channel) scale.

For instance, in the case of the total mass flow of two adjacent core channels at positions  $x = 15$ ,  $y = 11$ ,  $z = 6$  and  $x = 15$ ,  $y = 12$ ,  $z = 6$ , (in a  $X$ - $Y$  radial map of fuel assemblies and at the axial level 6) in the time interval between 235 s and 240 s as shown in Figure 17, the results of the FFT analysis are presented in Figure 18. The left-hand side plot shows the mass flow rate as an input feedback signal in ( $x = 15$ ,  $y = 11$ ,  $z = 6$ ), with an average value about 4.3 kg/s, but with considerably higher oscillation amplitudes if compared to the mass flow rate in ( $x = 15$ ,  $y = 12$ ,  $z = 6$ ), which shows an average value of about 5.4 kg/s on the right-hand side plot.

The FFT is applied separately to the unprocessed input signals and the results of the spectral analysis are shown in Figure 18. The analysis of the plots in Figure 18 shows that the amplitudes for an oscillation frequency of  $f = 0$  Hz (non-oscillatory component) is the one governing the time changes of the signal. The higher average value observed in the case of the channel on the right-hand side ( $x = 15$ ,  $y = 11$ ,  $z = 6$ ) results in a higher amplitude of the spectral output at  $f = 0$  Hz. The offset and a polynomial fitted to the slope, as shown in Figure 19, are subtracted from the input signals and the processed input signals are presented in Figure 20 (processed signal). These signals will provide the time-series for the FFT spectral analysis of the signal in both cells.

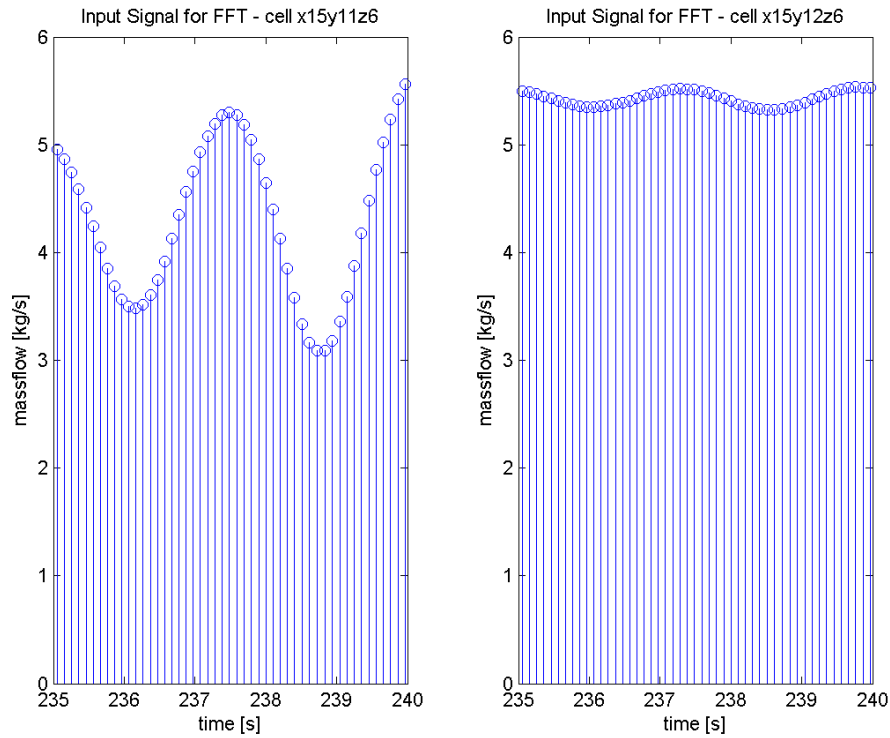


**Figure 17: Input signals of two adjacent cells in a 3-D x-y-z model of the BWR core during a feedwater transient event**

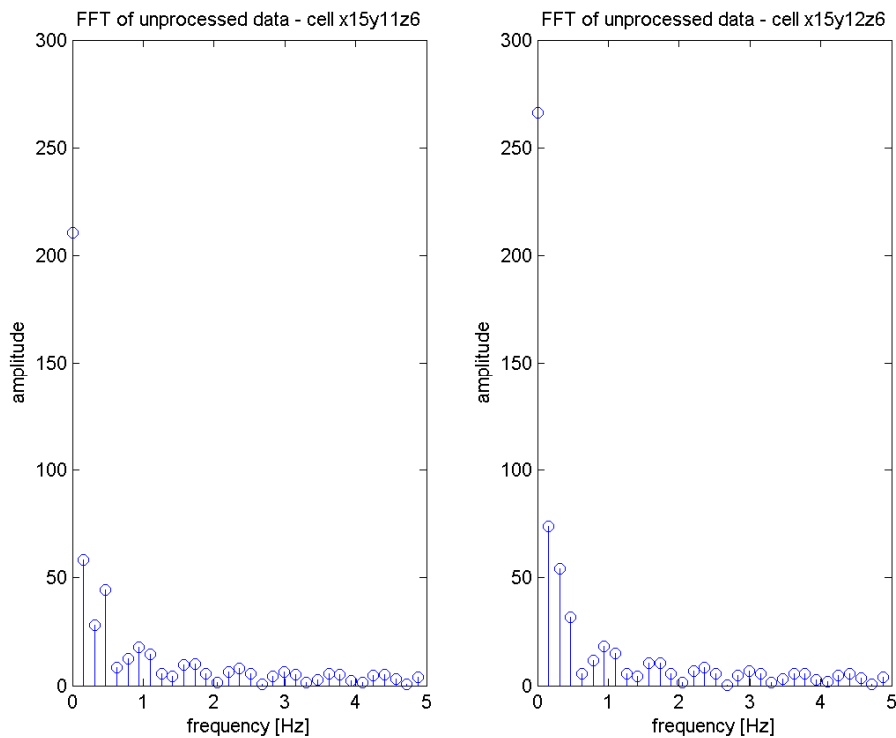


**Figure 18: Spectral analysis of the unprocessed mass flow rate signals for the two the adjacent core cells of Figure 17**

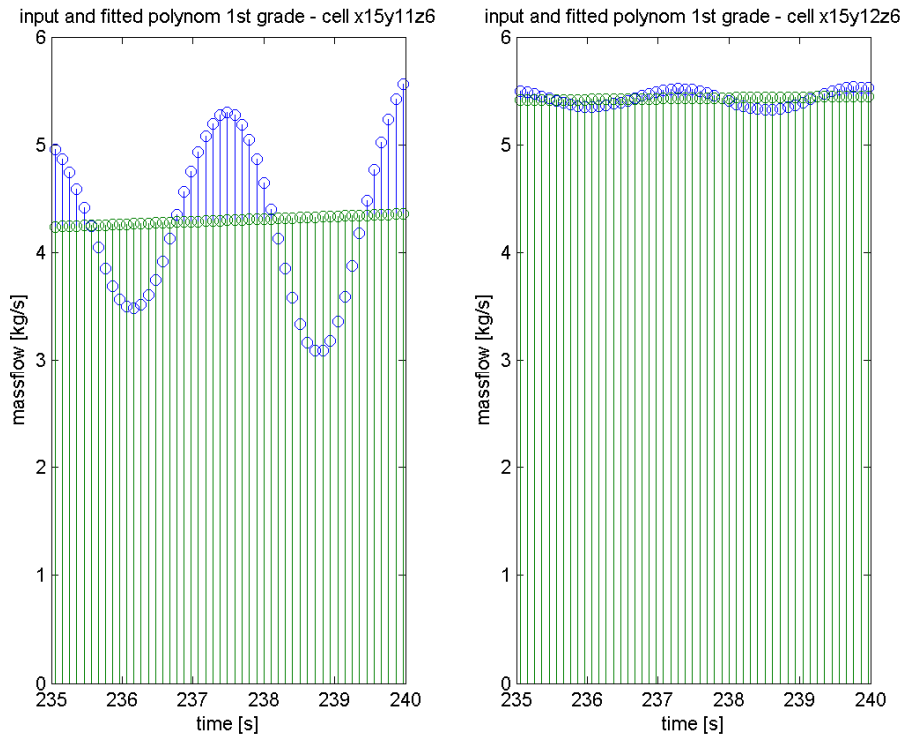


**Figure 19: Identification of the oscillatory and non-oscillatory part of the mass flow rate signals shown in Figure 17. The 1<sup>st</sup> order fitting shows the growing trend of the mass flow rate in both cells and indicates the faster variation of the one corresponding to (x = 15, y = 11, z = 6).**

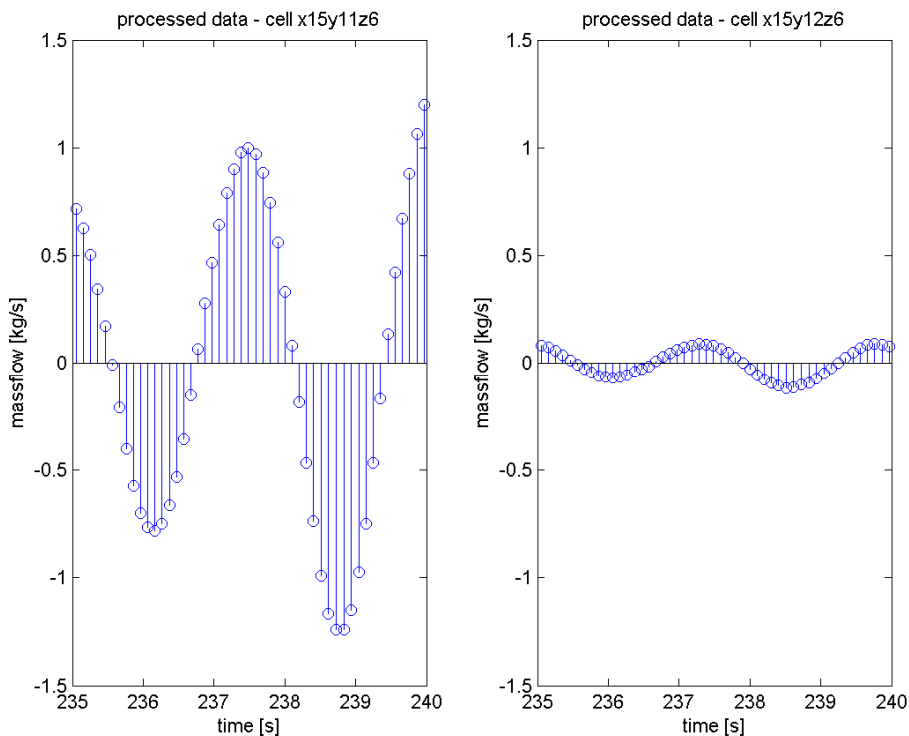


**Figure 20: Processed signals. Only the oscillatory part is considered for the spectral analysis.**

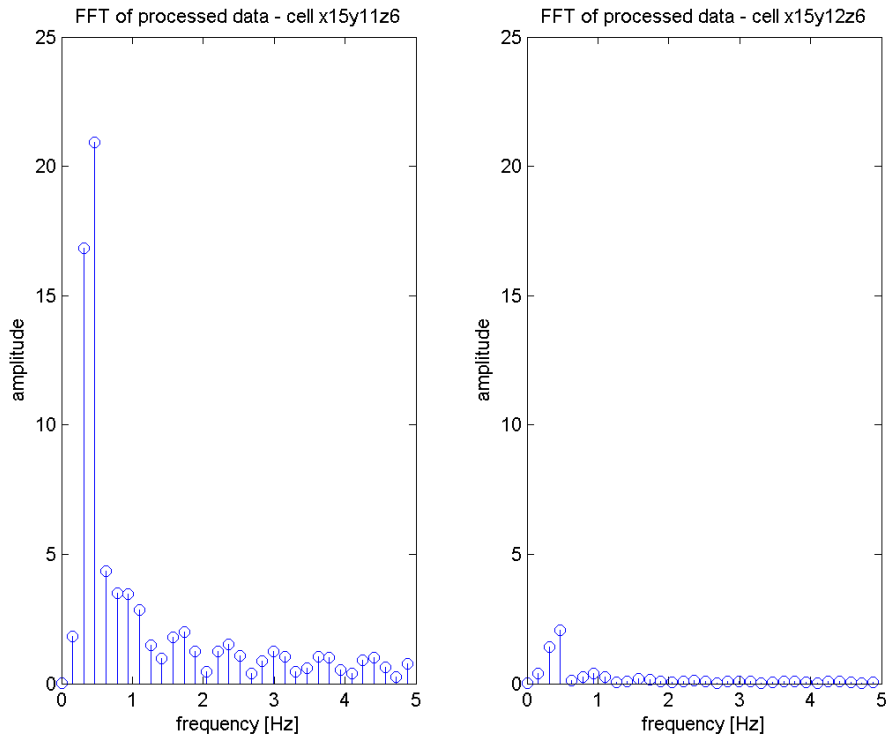


**Figure 21: Spectral analysis of the oscillation signal of two adjacent cells**

In Figure 21 one can see the result of the spectral analysis of the input signals reduced to their oscillation component. There is in both cases a maximum of amplitude for the characteristic frequency of about 0.5 Hz, but with clearly different values. In spectral analysis, the magnitude of the amplitude for a given frequency represents the weight of this frequency in the oscillatory behavior of the signal. We can interpret that in cell ( $x = 15$ ,  $y = 11$ ,  $z = 6$ ) a very large part of the contribution to the oscillations is caused by the 0.5 Hz component, and the oscillations in this cell is much stronger than those in the adjacent cell ( $x = 15$ ,  $y = 12$ ,  $z = 6$ ).

The preceding example of application is focused on two individual adjacent computational cells, but following a similar approach, an entire flow channel (or fuel assembly) of a complete axial level of the core can also be studied. In this manner, one can analyze the influence of feedback mechanisms in the radial direction, as well as in the axial direction.

Next, results for an entire axial core level are shown as an example of this application. The results, as those presented above, are taken from [27].

The spectral analysis extended to a core level permits a relative comparison of the oscillating contribution for each flow channel and allows the identification of those with a stronger influence on the core variable of interest, e.g. power. Thus, Figure 22 displays one radial plane of the complete core and Figure 23 gives an enlarged view of the central section of the core. Figure 24 shows the results for one axial section.

These are the steps to perform the analysis:

- (1) The analysis spans a certain time interval of interest during the transient. For this time, the signal variables can be read from the output file of the simulation. The length of the time interval (or time frame) length is freely selectable but must be adjusted to the system frequency and to the physical characteristics of the signal and transient.
- (2) The offset and the slope of the signal must be subtracted from the signal so that only the oscillatory part of it remains. The offset and slope are a result of system wide responses to feedback mechanisms, and they do not carry information about the signal oscillation, only time-

trends. All signals to be included in the analysis are thus normalized and they can be compared after the spectral decomposition.

- (3) The FFT is used to perform the spectral decomposition of the processed signals which yield the amplitude and frequency plots. The amplitudes observed in the frequency spectra are equal to the height of the amplitudes in the time domain for each specific Fourier series component.
- (4) Because of the normalization of this method, the interpretation of the spectral output shows that a computational cell with a high signal amplitude has a high oscillatory component compared to a cell with a lower amplitude and a lower oscillation component.
- (5) If the output of the spectral analysis shows a significant peak for a certain frequency, it can then be interpreted as this frequency being the dominant part of the signal. From a qualitative point of view, a spectrum with no outstanding peaks is produced in the case that no dominating frequency is driving the oscillations, and the signal can be considered as damped.

This procedure can be used for the analysis of oscillating signals at any local position in the core and for any kind of core variables, such as power, mass flow, density, void fraction, etc. The study can be carried out in any radial direction (Figure 22) or axial direction (Figure 24).

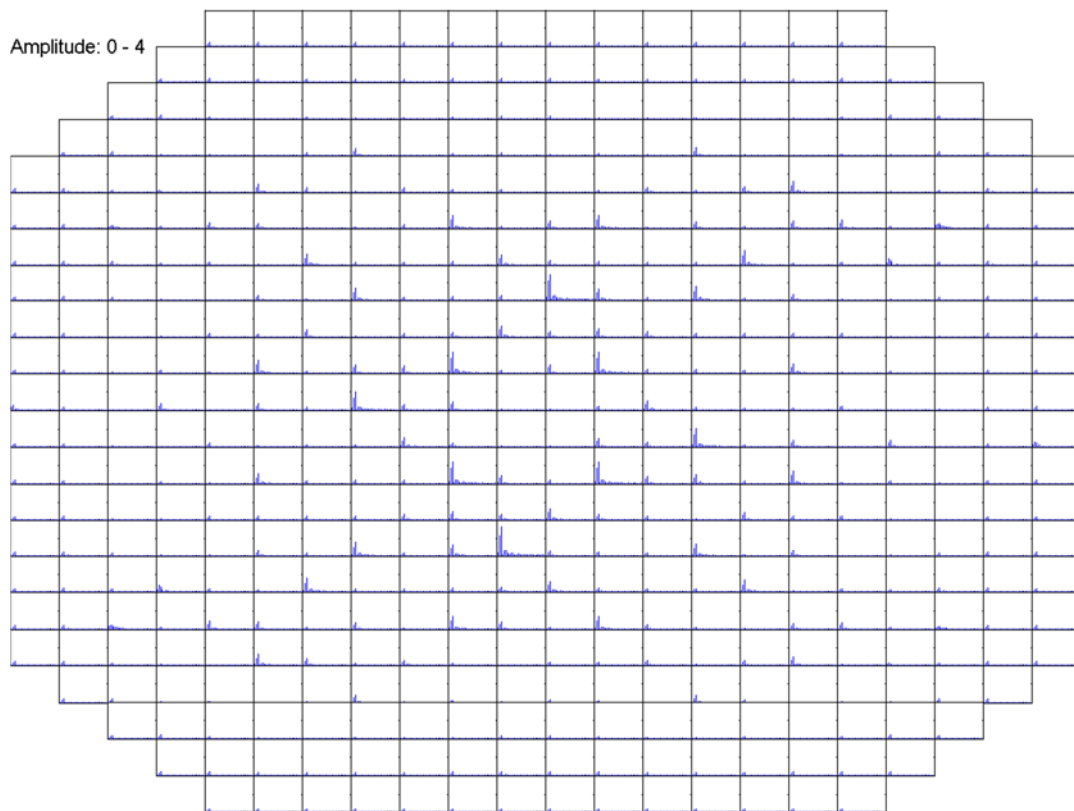


**Figure 22: Radial spectral analysis of the mass flow rate signal for core level 6.  
Each cell has an amplitude spectrum.**

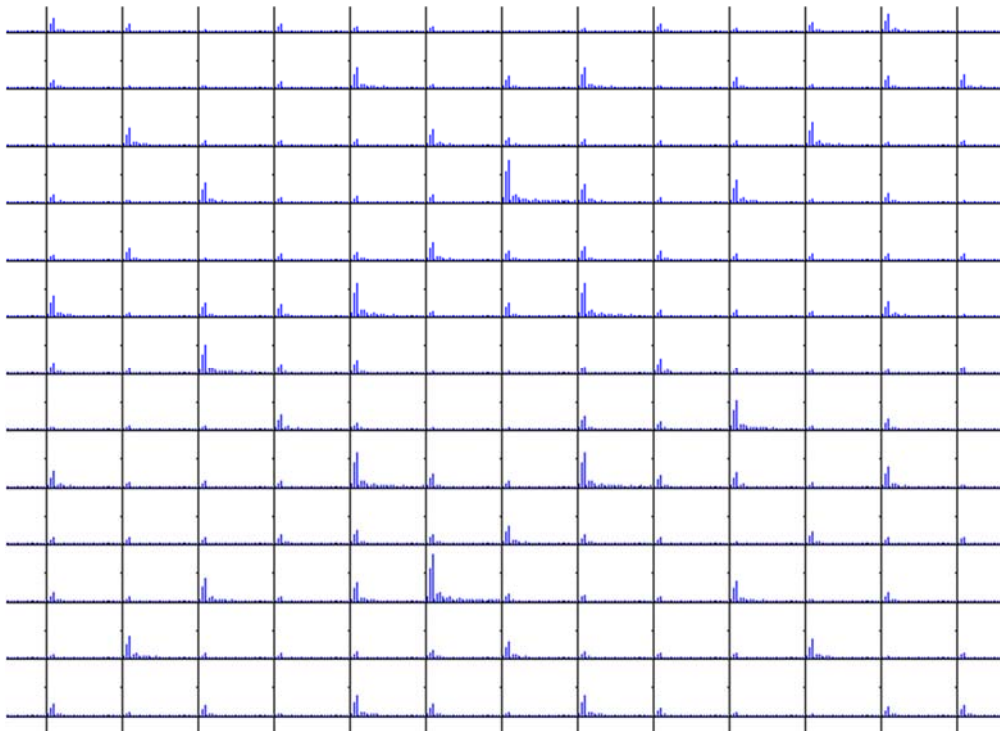


**Figure 23: Expanded central section of Figure 22. The cells (eventually fuel assemblies) driving the oscillatory feed-back behavior in the core are clearly identified by the high amplitudes about the 0.5 Hz frequency. Other fuel assemblies contribute much less or not at all to the power oscillations observed.**

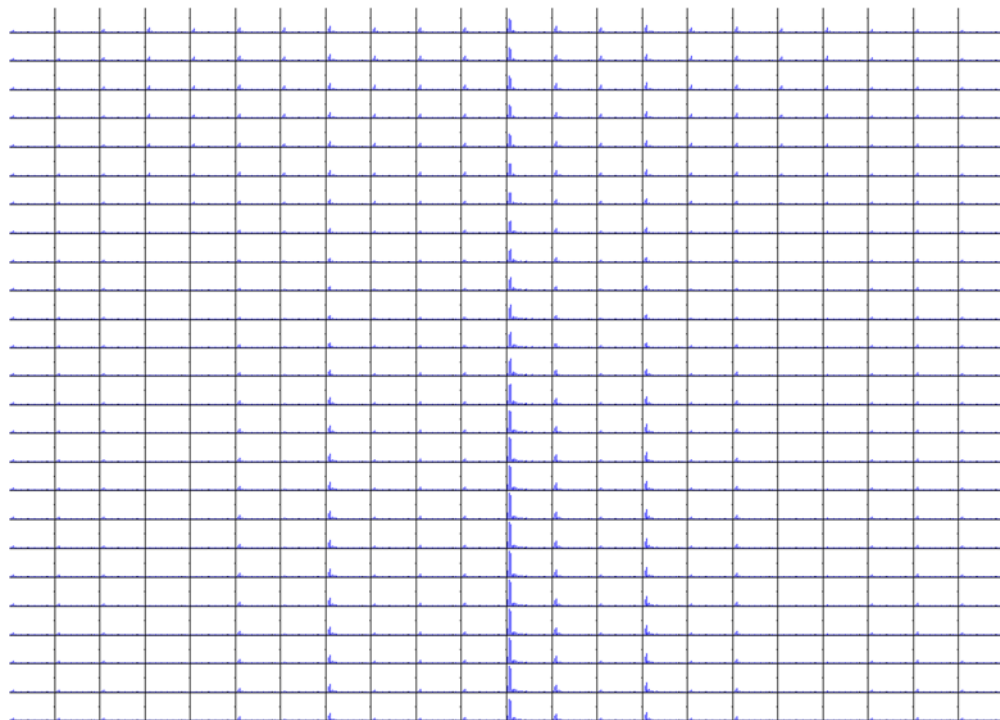


**Figure 24: Axial amplitude spectra for the fuel assemblies in an X-Y central core plane. The large influence of the central channel on the power oscillations, which are driven by the oscillations in mass flow rates, is clearly seen.**

### 3.4 Phase Shift Determination between Oscillating Parameters

The behavior of local signals relative to each other can shed light on their coupled influence. Figure 25 shows the time trends and their normalized oscillatory component for three core variables. The first column represents the total reactor power, the middle and the right column the total mass flow rates of two different channels. A phase shift relative to each other is clearly seen already in the time plots and in the processed plots.

The procedure described above has been performed with a MATLAB based tool developed at the Chair of Nuclear Engineering at TUM in the context of the work reported in [27]. The spectral analysis yields Figure 26 and Figure 27. In the amplitude plots of Figure 26 the maximum absolute value of the amplitude is determined and marked with a red color. The maximum value identifies the dominant frequency in the signals. Figure 26 also shows the corresponding phases in radians for each signal. The reactor power signal is used as a reference and the third row of Figure 27 shows the phase shifts, calculated by subtracting the phase of the reference signal from the phase of each signal. With the use of the reference phase, the phase shift of each signal is normalized, and the phase shifts of the signals are then comparable.

In order to verify the procedure, the Inverse Fast Fourier Transform (IFFT) is used to obtain the dominant signal component from the frequency domain in the time domain using the MATLAB function  $Y = \text{ifft}(X)$ . The first row of Figure 27 shows the inversely transformed signals (green lines) versus the original signals (blue lines). The reconstructed signals are very close to the original signals with respect to the frequency and the phase, thus showing the consistency of the methodology (one must remember that the spectral analysis is done on processed signals which only represent the oscillatory component for the largest amplitude, not the actual value of the signals as shown in the blue lines in which all amplitudes are included).

In this example a signal time frame of 14 seconds is shown. For the analysis of a transient, where the signals change over time, it is an advantage to use very short time frames and analyze one time-frame after another in order to investigate changes of the phase of each analyzed signal. It was found that a time frame length shorter than five seconds leads to insufficient amount of values to perform an accurate spectral analysis. As the oscillation frequency is about 0.4 Hz, a time frame length of 5 seconds corresponds to 2 complete oscillation cycles. With such a small number of oscillations, the spectral decomposition is not accurate enough.

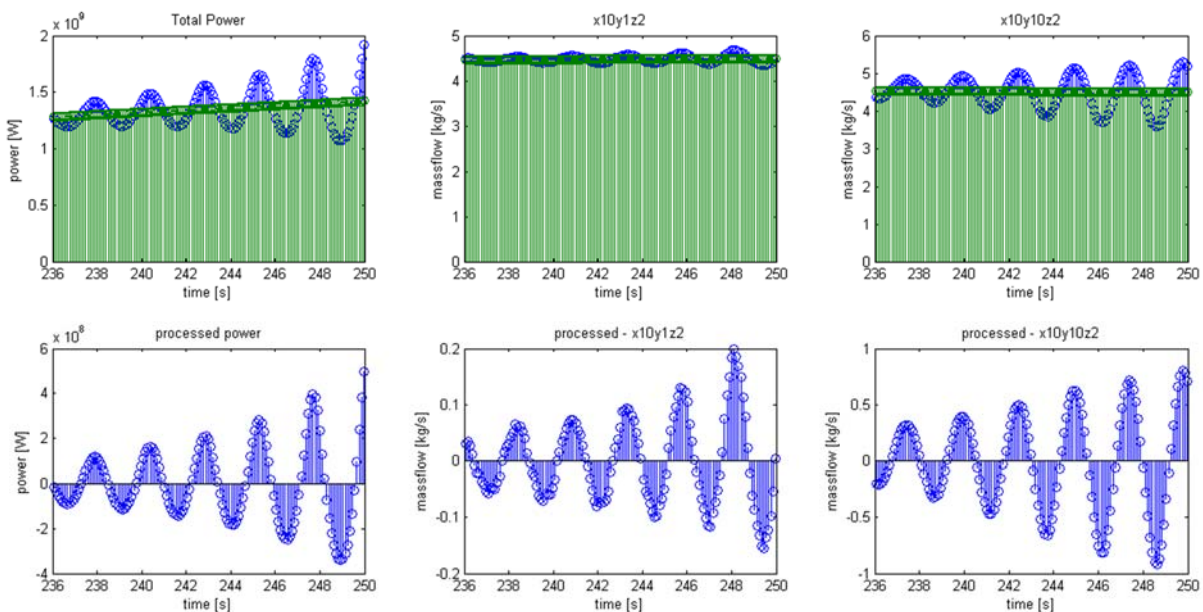


**Figure 25: Time dependent signal and processing for three reactor feed-back coupled variables. Above: full values. Below: processed signal with only the oscillatory components.**

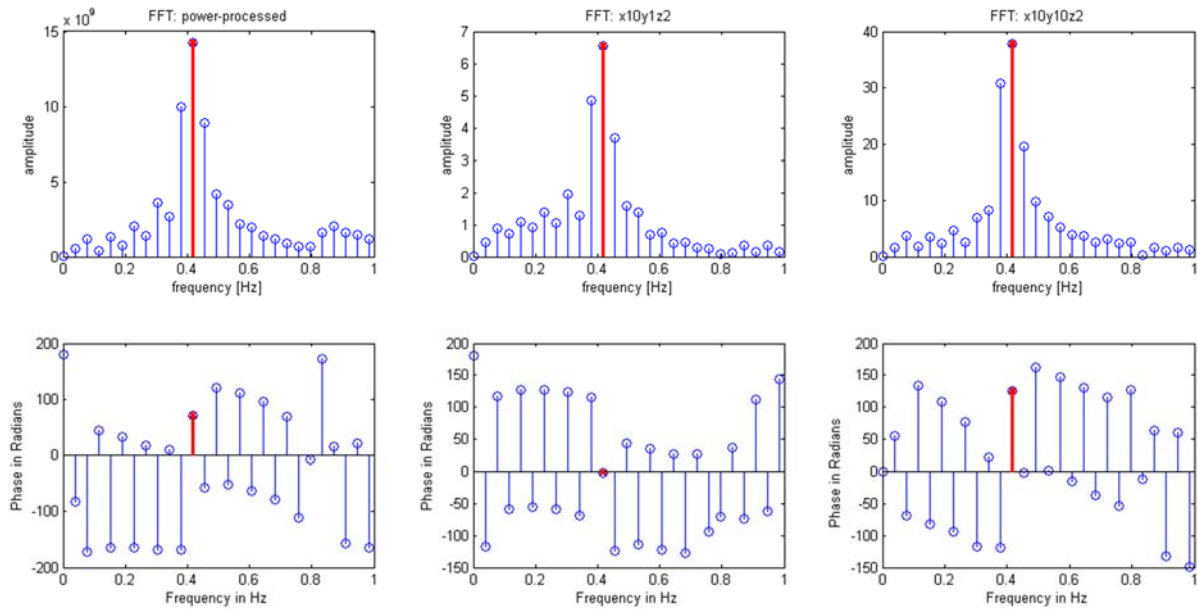


**Figure 26: Spectral analysis of the three signals in Figure 25. A dominant frequency in the three cases show a clear coupling between the power and the mass flow rate with a frequency about 0.4 Hz for the dominant channels. The phase shifts (see figure below) show that the oscillations are happening through time-delayed feedback mechanisms as is expected physically in these types of oscillations.**

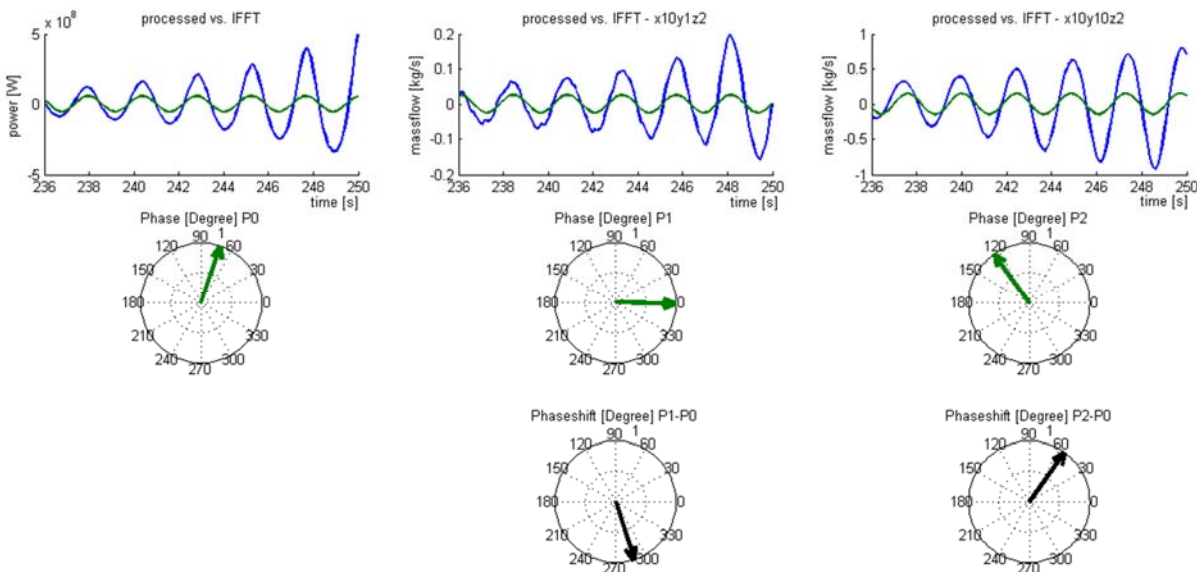


**Figure 27: Time domain reconstruction of the signals. The plots above show the consistency of the methodology. The plots below show the phase shifts for the most influential frequency at about 0.4 Hz.**

The phase-shift comparison, which gives information on the influence between the signals (e.g. due to physical coupling), is only rigorously useful if signals have a sinusoidal shape. If they contain a large amount of noise, then a phase shift calculation may not be helpful. The results of the spectral analysis would have low amplitude peaks and a broad overall shape that may not highlight a given frequency as dominant. The elimination of the noise by applying some filtering procedure may result in a periodic sinusoidal signal which can then be treated in the manner described above.



## 4 Conclusions

This report presented: 1) the basic methodology for uncertainty propagation and sensitivity analysis that was developed in the context of the CORTEX project; and 2) a methodology based on spectral/frequency decomposition for the analysis of oscillatory phenomena in nuclear reactors.

The methodology for uncertainty and sensitivity analysis is specifically tailored on neutron noise simulations. For the verification of the developed framework, a test was carried out as follows. Nuclear data were generated with the code Serpent for the zero-power research reactor CROCUS in such a manner that the uncertainties associated with relevant nuclear and geometric properties of the reactor were considered. A hypothetical case of an absorber of variable strength in CROCUS was simulated with the neutron noise simulator CORE SIM and the impact of the uncertainties on the calculated neutron noise was evaluated with the methodology.

The main outcomes of this study can be summarized as below.

- The proper steps for the uncertainty quantification and the sensitivity analysis are identified and implemented from the cross-section generation to the core analysis of neutron fluctuations.
- The uncertainty propagation is performed with two different approaches and the results are compared in terms of conservatism related to the magnitude and phase of the oscillations.
- The correlation-based approach and the variance-based approach are considered for the sensitivity analysis so that the most affecting parameter on the neutron noise can be identified.
- The use of variance-based sensitivity analysis is shown as the more appropriate approach in case of analyzing the neutron noise behavior.

However, still there is room for improvement by changing the core modelling for the code calculation, increasing the quality of surrogate modelling, modifying the way of uncertainty treatment, and so on. These items will be considered in the future studies and the quality of the methodology is expected to be enhanced accordingly.

Additionally, the established methodology will be considered in other type of reactors (both research and power reactors) with different types of neutron noise sources. This will enable the developed methodology to be versatile especially for the analysis of the neutron flux oscillations.

The methodology based on spectral/frequency decomposition for the analysis of oscillatory phenomena in nuclear reactors was developed at the Chair of Nuclear Engineering of the TUM in the course of a PhD and resulted in a software package written in MATLAB script capable of performing the analyses described. The choice of reactor variables depends on the particular application and can be adapted to the study of neutronic oscillations in the context of the CORTEX project for time-dependent simulations of neutron oscillations.

Only the extraction of core data needs to be tailored to the code system used in the simulations.

The full application of the methodology to an actual core, which can be read in [27], allows for a full core determination of the spectral and phase plots for every computational cell in the core and for any radial plane or axial flow channel or fuel assembly. This information permits the identification of the most influential oscillation inducing channels (fuel assemblies) and their influence (through the dominant frequencies and phase shifts) on core variables such as neutron flux and power.

Since we will use Fourier transform based approach to observe the trends of the amplitude and the phase in the core, the usage of an analysis code in time domain is required. In this context, we should determine a proper analysis code for further analysis. Plus, we should be able to obtain the basic input files where the target reactor model is implemented in advance so that we can modify and run them through the target code immediately.

## 5 References

- [1] A. Saltelli, K. Chan, and E.M. Scott, editors, "Sensitivity analysis." Wiley Series in Probability and Statistics. Wiley, 2000.
- [2] J. Leppänen, "Serpent-a Continuous-energy Monte Carlo Reactor Physics Burnup Calculation Code," User's Manual, VTT Technical Research Centre of Finland, 2015.
- [3] C. Demazière, "CORE SIM: A multi-purpose neutronic tool for research and education," Annals of Nuclear Energy, vol. 38, pp. 2698-2718, 2011.
- [4] V.Lamirand, M.Hursin, P.Frajtag and A. Pautz, "Future Experimental Programmes in the CROCUS Reactor." RRFM/IGORR 2016, Berlin, Germany, March 13-17, 2016.
- [5] David J.Diamond, "Experience Using Phenomena Identification and Ranking Technique (PIRT) for Nuclear Analysis," PHYSOR-2006 Topical Meeting, Vancouver, Canada, September 10-14, 2006.
- [6] A. Rais, "SERPENT code few-group constants generation for the CROCUS reactor," CORTEX project internal technical report, 2018.
- [7] J. Kirchner, "Data Analysis Toolkit #5: Uncertainty Analysis and Error Propagation," (PDF) Berkeley Seismology Laboratory, University of California, Retrieved 22 April 2016.
- [8] M. Kloos and E. Hofer, "SUSA - PC, a personal computer version of the program system for uncertainty and sensitivity analysis of results from computer models, version 3.2," user's guide and tutorial, Gesellschaft für Anlagen- und Reaktorsicherheit, Garching, Germany, August 1999.
- [9] S. Deviant Mat, "The Practically Cheating Statistic Handbook," Create Space Independent Publishing Platform, 2010.
- [10] W. J. Conover, "Practical Nonparametric Statistics," 3<sup>rd</sup> ed., John Wiley & Sons, New York, 1980.
- [11] Setpoint for Safety-Related Instrumentation, U.S. NRC Regulatory Guide 1.105, Rev.3, Dec. 1999.
- [12] Best Practice Guidelines for the use of CFD in Nuclear Reactor Safety Applications, NEA/CSNI, May. 2007.
- [13] H. Ackermann and K. Abt, "Designing the Sample Size for Non-parametric, Multivariate Tolerance Regions," Biometrical Journal, vol. 26, pp. 723-734, 1984.
- [14] D. F. da Cruz, D. Rochman and A. J. Koning, "Propagation of nuclear data uncertainty for a control rod ejection accident using the total Monte-Carlo method," PHYSOR 2014, Kyoto, Japan, September 28-October 3, 2014.
- [15] J. Toby Mordkoff, The Assumption(s) of Normality, lecture material of psychology department at Iowa University, 2000.
- [16] S. N. Lophaven, H. B. Nielsen, J. Søndergaard, „DACE: A Matlab Kriging Toolbox, version 2.0," Technical Report IMM-TR-2002-12 in Technical University of Denmark, 2002.
- [17] O. Borries, "Surrogate Modelling using DACE," Bachelor of Science Thesis IMM-B.Sc.-2009-8, Technical University of Denmark, 2009.
- [18] Y. Gan et al., "A comprehensive evaluation of various sensitivity analysis methods: A case study with a hydrological model," J. Environmental Modelling & Software, vol. 51, pp. 269-285, 2014.
- [19] M. Mukaka, "A guide to appropriate use of Correlation coefficient in medical research," J. Malawi Med., vol. 24(3), pp. 69-71, 2012.
- [20] I. M. Sobol', "Global sensitivity analysis indices for nonlinear mathematical models and their Monte Carlo estimates," Mathematics and Computers in simulation, vol.55, pp. 271-280, 2001.
- [21] I. M. Sobol', "Sensitivity analysis for non-linear mathematical models," Mathematical Modelling and Computational Experiment, vol. 1, pp. 407-414, 1993.
- [22] B. Iooss and P. Lemaître, "A Review on Global Sensitivity Analysis Methods," Operations Research/Computer Science Interfaces Series, vol. 59, 2014.
- [23] A. Saltelli, et al., "Variance based sensitivity analysis of model output. Design and estimator for the total sensitivity index," Computer Physics Communications, vol. 181, pp. 259-270, 2010.
- [24] M. J. W. Jansen, "Analysis of variance designs for model output," Computer Physics Communications, vol. 117, pp. 35-43, 1999.



- [25] X. Sun, S. Roberts, B. Croke, A. Jakeman, "A comparison of global sensitivity techniques and sampling method," 22<sup>nd</sup> International Congress on Modelling and Simulation, Hobart, Tasmania, Australia, December 3-8, 2017.
- [26] H. Wan, et al., "Sensitivity and Interaction Analysis Based on Sobol' Method and Its Application in a Distributed Flood Forecasting Model," *Water*, vol. 7, pp. 2924-2951, 2015.
- [27] S. Walser, "Development and Application of a Fourier Transform-based Methodology for the Identification of Instability in Boiling Water Reactors at a Local Scale," PhD thesis, Technical University of Munich, 2017.